SIZE AND COMPOSITION MODULATED SUPERLATTICES OF SILICON BASED NANOWIRES

A THESIS

SUBMITTED TO THE PROGRAM OF MATERIAL SCIENCE AND NANOTECHNOLOGY

AND THE INSTITUTE OF ENGINEERING AND SCIENCE

OF BILKENT UNIVERSITY

IN PARTIAL FULFILLMENT OF THE REQUIREMENTS

FOR THE DEGREE OF

MASTER OF SCIENCE

By

Seymur Cahangirov

July, 2008

I certify that I have read this thesis and that in my opinion it is fully adequate, in scope and in quality, as a thesis for the degree of Master of Science.

Prof. Dr. Salim Çıracı (Advisor)

I certify that I have read this thesis and that in my opinion it is fully adequate, in scope and in quality, as a thesis for the degree of Master of Science.

Prof. Dr. Engin Akkaya

I certify that I have read this thesis and that in my opinion it is fully adequate, in scope and in quality, as a thesis for the degree of Master of Science.

Assist. Prof. Ramazan Tuğrul Senger

Approved for the Institute of Engineering and Science:

Prof. Dr. Mehmet B. Baray
Director of the Institute Engineering and Science

ABSTRACT

SIZE AND COMPOSITION MODULATED SUPERLATTICES OF SILICON BASED NANOWIRES

Seymur Cahangirov
M.S. in Material Science and Nanotechnology
Supervisor: Prof. Dr. Salim Çıracı
July, 2008

Mechanical properties, atomic and energy band structures of bare and hydrogen passivated Si_nGe_n nanowire superlattices have been investigated by using first-principles pseudopotential plane wave method. Undoped, tetrahedral Si and Ge nanowire segments join pseudomorphically and can form superlattice with atomically sharp interface. Upon heterostructure formation, superlattice electronic states form subbands in momentum space. Band lineups of Si and Ge zones result in multiple quantum wells, where specific states at the band edges and in band continua are confined. The electronic structure of the nanowire superlattice depends on the length and cross section geometry of constituent Si and Ge segments. Also we showed that hydrogen saturated silicon nanowires of different diameters having different band gaps can form stable junctions. Superlattices formed by the periodically repeated junctions of silicon nanowire segments having different lengths and diameters exhibit electronic states which can be confined in regions having either narrow or wide parts of superlattice. A point defect, such as a missing atom or substitutional impurities with localized states near band edges can make modulation doping possible. Since bare Si and Ge nanowires are metallic and the band gaps of hydrogenated ones varies with the diameter, these superlattices offer numerous options for multiple quantum well devices with their leads made from the constituent metallic nanowires. Finally, we have considered the junction between bare and hydrogenated nanowires to realise metal-semiconductor heterostructure. We have treated this heterostructure within the supercell geometry and deduced the formation of Schottky barrier. We have shown that Si and Ge nanowires can bring about a novel concept in nanocircuit, where interconnects, devices etc are produced on a single rode.

Keywords: ab initio, density functional theory, nanowire, superlattice.

ÖZET

BÜYÜKLÜK VE ŞEKİL MODÜLASYONLU SİLİSYUM TABANLI NANOTEL SÜPERÖRGÜLER

Seymur Cahangirov
Malzeme Bilimi ve Nanoteknoloji , Yüksek Lisans
Tez Yöneticisi: Prof. Dr. Salim Çıracı
Temmuz, 2008

Hidrojenle doyurulmuş Si_nGe_n nanotel süperörgülerin mekanik özellikleri, atomik ve enerji band yapısı temel prensiplerle, pseudo potansiyel ve düzlemsel dalga yöntemiyle incelendi. Katkısız, tetrahedral Si ve Ge nanoteller yapay olarak birleşebilmekte ve atomik seviyede keskin arayüzlü süperörgü oluşturabilmektedir. Heteroyapı oluşumuyla birlikte, süperörgüye ait elektronik durumlar momentum uzayında bant oluşturmaktadır. Si ve Ge bölgesindeki bantların sıralanması sonucu çoklu kuantum kuyuları oluşmakta ve bazı durumlar bu kuyularda yoğunlaşmaktadır. Ayrıca, farklı çaplara sahip hidrojenle doyurulmuş silisyum nanotellerin bağlanarak kararlı yapı oluşturduğu gözlemlenmiştir. Farklı çap ve uzunluktaki silisyum nanotellerin periyodik olarak birleşmesi sonucu oluşan süperörgüler ilginç elektronik özellikler göstermektedir. Bazı elektronik durumlar kalın ya da ince kısımda yoğunlaşabilmektedir. Eksik bir atom ya da yerine başka atomun geçmesi sonucu oluşan noktasal bozukluklar bant kenarında yerel durumlara neden olmakta ve bu da modülasyon katkılamayı mümkün kılmaktadır. Çıplak Si ve Ge nanotellerin metalik özellik taşıması ve hidrojenle doyurulanların yasak enerji aralığının içerik ve yarıçapa göre değişmesi bu yapıların çoklu kuantum kuyusu aygıtı olarak kullanılabileceğini ve bağlantıların metalik nanotellerle yapılabileceğini göstermektedir. Son olarak, çıplak ve hidrojenle doyurulmuş silisyum nanotellerin birleşmesiyle oluşan metal-yarıiletken heteroyapılar incelendi. Bu heteroyapılar süperhücre geometrisiyle ele alındı ve Schottky bariyeri oluşumu sonucuna varıldı. Nanoelektronikte yeni bir konsept olarak, Si ve Ge nanotellerin kullanımıyla tek tel üzerinde bağlantılar, devreler ve s. yapımının mümkün olduğu gösterildi.

Anahtar sözcükler: ab initio, yoğunluk fonksiyonu teorisi, nanotel, süperörgü.

Acknowledgement

I would like to express my deepest gratitude to my supervisor Prof. Dr. Salim Çıracı for his priceless guidance. He is the only person I know, who mixes administration and politeness in perfect ratios.

I would like to thank Dr. Engin Durgun for sharing his life and research experience as a friend and scientist.

I would like to thank Dr. Haldun Sevinçli, who always had answers to my science questions.

I would like to thank my friends and research partners Mehmet Topsakal, Can Ataca, Erman Bekaroğlu and Hasan Şahin for wonderful time I had with them during research. Also I would like to thank all my friends in the Institute of Material Science and Nanotechnology and Department of Physics.

I would like to thank people of Azerbaijan where I have grown up and hospitable people of Turkey where I had my undergraduate and graduate education.

Special thanks go to my parents, my brother and my sister and all other relatives support of whom I always felt behind me.

Finally I would like to thank and dedicate this thesis to my wife Naide for sharing her life with me.

Contents

List of Figures

List of Tables

Chapter 1

Introduction

Superlattices are heterostructures formed by periodically varying layers of two or more substances. Building blocks of superlattices can be either metals or semiconductors. Planar semiconductor superlattices were first grown in 1970's and metallic ones in 1980. In planar semiconductor superlattices, band gap varies periodically in direct space along direction perpendicular to the layers. Because of this geometry, minibands are formed in momentum space perpendicular to the layers. This results in unusual electronic functions for novel devices. Field effect transistors (FETs), photodetectors, light emmiting diodes (LEDs), quantum cascade lasers are few examples of these novel applications.

Nowadays, with the help of new growth techniques one-dimensional (1D) nanowire superlattices are synthesized. These nanowire superlattices have potential to combine functions of nanowires and superlattices. The crucial question here is whether superlattice geometry conserves conventional properties when layers with large areas are diminished to nanosize. This will result in LEDs, FETs and other superlattice devices which are not only compatible with well known semiconductor technology but also increase information capacity in enormous range.[1]

One of the most promising applications of nanowires are termoelectric devices.[2] As indicated by Maria Telkes [3], in her 1947 paper, bulk silicon is

not efficient as a termoelectric device. This is because silicon is a good heat conductor and it can't prevent heat diffusion, i.e. temperature gradient along the device could not be maintained. However when cross-section is reduced to nanosize thermal conductivity is reduced by 100 times relative to its bulk counterpart. This effect takes place because heat carrying phonons, electrons and holes are faced with obstacles like nanowire edges. Nanowire geometry not only reduces thermal conductivity but also helps to adjust other parameters affecting thermoelectric efficiency like Seebeck coefficient and electrical resistivity. Recently two independent experimental works [4, 5] indicate that silicon nanowires with cross-section radius of 20-50 nm can be managed to give thermoelectric efficiencies comparable with commercial bismuth-telluride semiconducting thermodevices.[2]

Fluorescence in nanowires is also an interesting research area.[6] According to work by Protasenko et al. [7] fluorescence of CdSe nanowires can be controlled by electric field which opens a room for possibility of mobile charge carriers. This finding can open a broad application area in nanoelectronics.

It is also possible to combine semiconducting nanowires with metallic carbon nanotubes in order to get a miniaturized version of conventional Schottky diodes. Hu and Ouyang et al .[8] have synthesized silicon nanowire, carbon nanotube junctions in a catalytic growth procedure. It is shown that these junctions behave as a Schottky diode and what is more interesting is that they have similar zero-bias junction barrier height as macroscopic metal/p-Si junctions, inspite of their nanosize.

Heterojunctions of compositionally modulated n- and p-type nanowires are also realised in several experimental studies. Gudiksen et al .[9] have synthesized compositionally modulated GaAs and GaP nanowires together with modulation doped n-Si/p-Si and n-In/p-In nanowires. Here GaAs gives strong luminescence but GaP does not. Authors claim that this property can be used for the design of an optical nano-barcode. Also they report light emmition, from modulation doped nanowires, as forward bias is applied. This is a realisation of nanoscale LED.

Core-shell geometry of nanowires were also investigated. Xiang et al. [10]

reported a realised nanowire field-effect transistor (NWFET) composed of a Si core and Ge shell geometry. They state that performance of Ge/Si NWFETs are of same order of magnitude with similar length carbon nanotube FETs. The importance of this result lies in difficulties of producing uniform semiconducting carbon nanotubes.

In summary, following subjects related to nanowires have been investigated experimentally and/or theoretically;

- Nanosized Thermoelectric Devices
- Polarized Nanoscale Light Emmiting Diodes (NLEDs)
- Nanosized Field Effect Transistors (NFETs)
- Optical Nano-Barcodes
- 1D Electron Waveguides
- Single Electron Devices (Quantum Computation)
- Multiple Quantum Well Devices
- Nano-Interconnects
- Nanosensors

1.1 Motivation

Because of interesting electronic structure they possess, conventional planar superlattices drew attention of both scientists and device engineers for past 30 years. During this period of time a new interdisciplinary field - nanotechnology emerged. Nanotechnology not only aims to reduce well known technology to nanoscale but also tries to explore the new application areas, taking advantages of the quantum world. While the two-dimensional heterostructures of semiconductors have a subject of active study leading to the discovery of interesting quantizations of

electrons in lower dimensionality and fabrication of exotic devices and quantum structures, analogous behaviors are expected to occur in nanowire heterostructures. In this thesis we show that one can preserve superlattice effects in size and compositionally modulated nanowires having diameters of only few nanometers range. We believe that this work will have a considerable impact in both science and device engineering community.

1.2 Organization of the Thesis

The thesis is organized as follows: Chapter 2 summarizes the basic properties and synthesis procedure of silicon and germanium nanowires and superlattices. Chapter 3 gives a brief theoretical background needed for our work. Chapter 4 includes results related to structural, electronic properties of compositionally modulated Si/Ge nanowire superlattices and electron confinement effects in these structures. Chapter 5 consists of results related to size modulated Si nanowire superlattices. Chapter 6 is about bare and hydrogenated silicon nanowire superlattice heterostructures. Finally, Chapter 7 summarizes and gives some conclusive remarks for this thesis.

Chapter 2

Silicon and Germanium Nanowires

Nanowires are materials having dimensions of order of nanometer along some plane of their bulk counterparts and grown perpendicular to that plane. Silicon nanowires were grown along [100], [110], [111] and [112] directions in several experimental works.[4, 5, 11] Bare nanowires have very reactive dangling bonds along their surface. These dangling bonds can be passivated by hydrogen, to prevent oxidation. Size of nanowires are defined by either number of atoms in the unitcell along the growth direction or by cross-sectional diameter. Generally this diameter is defined as highest distance between two atoms in the same layer. Although this definition is somewhat ambiguous, it gives an approximate picture for the reader. Core of the nanowires generally conserve bulk structure while surface is recostructed to minimize the total energy by reducing the number of dangling bonds. Nanowire superlattices are formed by joining two different types of nanowires and repeating this periodically. It is important to have a sharp interface between two adjacent parts of nanowire superlattices, i.e., they should be joined pseudomorphically. For Si and Ge nanowires it is possible because they have same bulk crystal structure and similar lattice constants. Wu et al. have synthesized Si/SiGe nanowire superlattice structure by using a hybrid technique which combines pulsed laser ablation and chemical vapor deposition.[12]

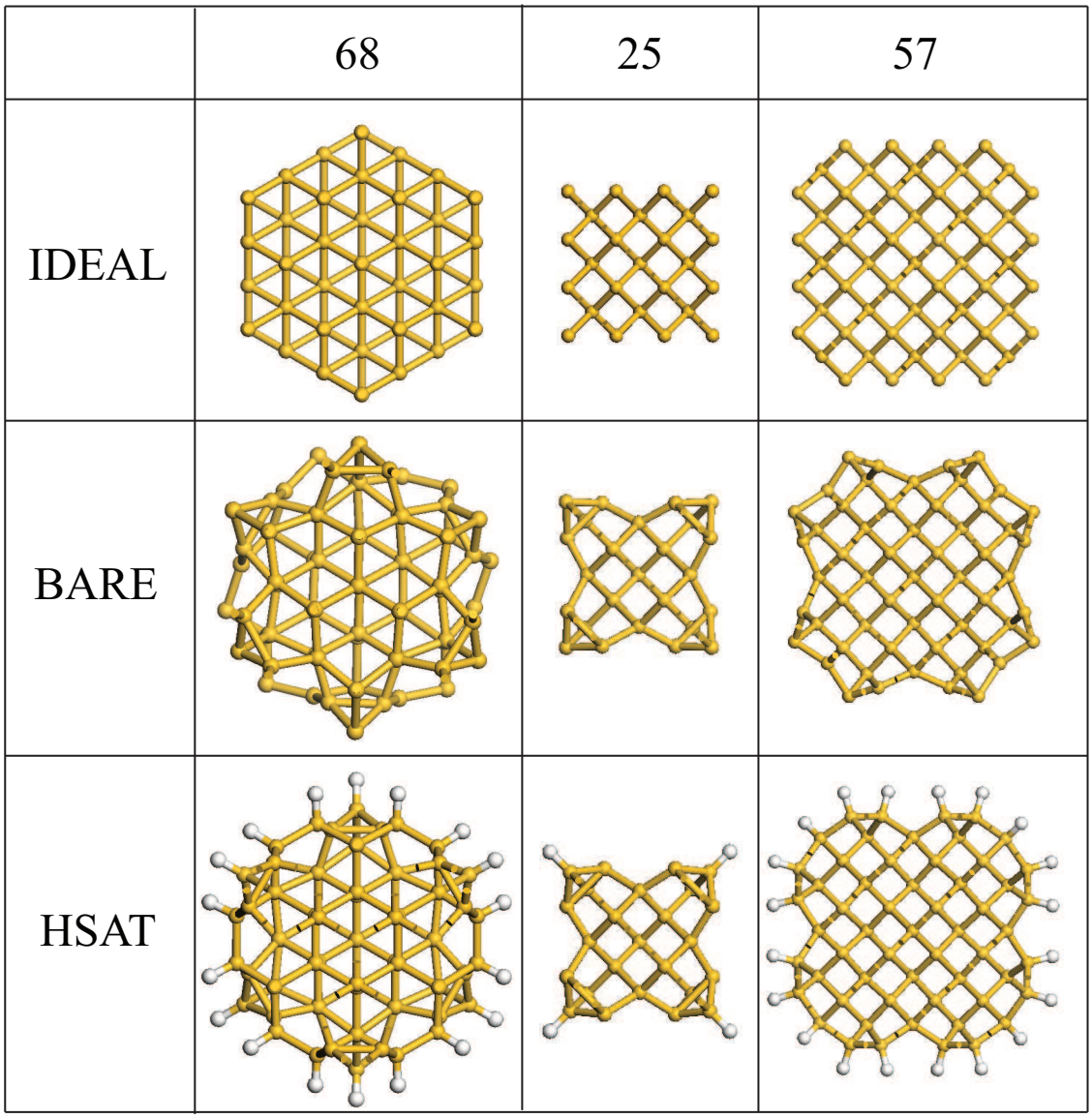

Figure 2.1: Ideal, bare and hydrogenated silicon nanowires are presented. Nanowires having 68 (25 and 57) atoms in a unit cell are cut along [111] ([100]) direction.

2.1 Structure

In ab initio calculations nanowires are generally cut from ideal bulk structure and then fully relaxed until they find a local minima. Then dangling bonds are saturated by hydrogen and structure is again relaxed. However some authors prefer hydrogenation of ideal structures at the beginning. Sometimes these two approaches give different results, but in our respect it is more suitable to choose first method. Fig. 2.1 shows cross-sectional view of silicon nanowires having 25, 57 and 68 atoms per unit cell. As seen here core of nanowires remains similar to ideal case while reconstructions occure at the surface. Surprisingly, sharp edges occure especially at the surface of Si_{25} nanowires. Normally we would expect round shapes to be prefered but this sharp structure allows dimerization along the surface and lowers the total energy.[13] Generally, cross-section of nanowires become smoother after hydrogenation. Structure of germanium nanowires are very similar to silicon nanowires, except longer bond distances. Since both nanowires have similar structure and lattice constant they can form atomically sharp interfaces. More detailed treatment of structural and mechanical properties of Si/Ge nanowire superlattices are left to Chapter 4.

2.2 Electronic Properties

Since core of the nanowires preserve bulk geometry, these atoms result in bulk-like electronic properties. However, surface states change the overall electronic behaviour fundamentally. Generally these states have higher dispersion and play important role in making bare nanowires metallic. Saturation of dangling bonds on the surface of silicon and germanium nanowire prevents these surface states and as a result we get a semiconducting nanowire. While bulk silicon and germanium have indirect band gaps, nanowires of silicon and germanium generally

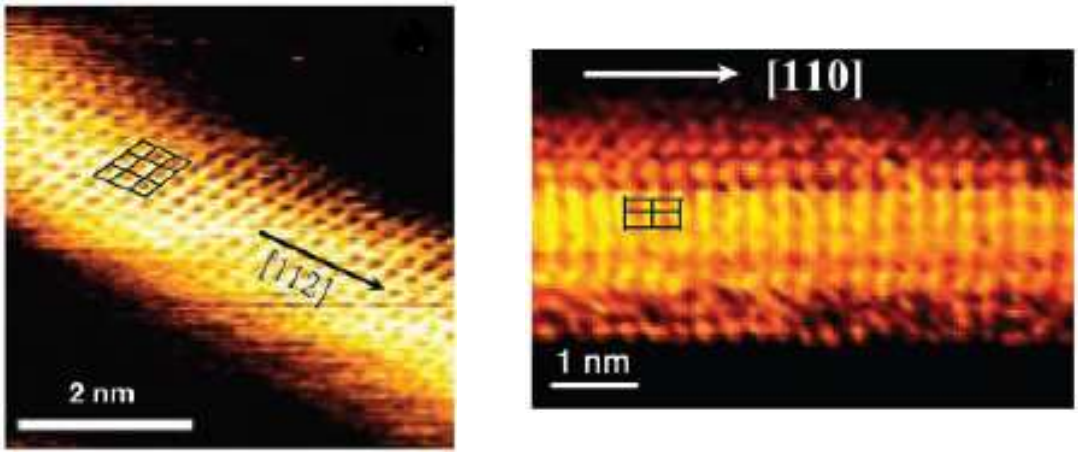

Figure 2.2: STM images of silicon nanowires grown along [112] and [110] directions, as given in the Ref. [11]

have direct band gaps what makes them potential candidates for optical devices.

2.3 Synthesis of Nanowire Superlattices

There are several ways to synthesize nanowires and nanowire superlattices. One way is to use, vapour-liquid-solid process with a metal catalyst, generally gold nanoparticles. In this method nanoparticles control the diameter of nanowires. This method gives good results for compositionally modulated nanowire superlattices. GaAs/GaP and InAs/InP nanowire superlattices were synthesized by this method with a diameter as small as 20 nm.[9, 14] Another way is to use superlattice nanowire pattern transfer method. Using this method one can adjust dimensions, impurity doping levels and crystallographic nature of silicon based nanowires.[4] Hybrid methods like one used in Ref. [12] also give good results for nanowire superlattices. Silicon nanowires fabricated by oxide-assisted growth method [11, 15, 16] are shown in Fig.2.2. These nanowires can have diameters as small as 1 nm.

Chapter 3

Theoretical Background

3.1 Density Functional Theory

The initial work on Density Functional Theory (DFT) was reported in two publications: first by Hohenberg-Kohn in 1964 [17], and the next by Kohn-Sham in 1965.[18] This was almost 40 years after Schrodinger (1926) had published his pioneering paper marking the beginning of wave mechanics. Shortly after Schrodinger‘s equation for electronic wave function, Dirac declared that chemistry had come to an end since all its content was entirely contained in that powerful equation. Unfortunately in almost all cases except for the simple systems like He or H, this equation was too complex to allow a solution. DFT is an alternative approach to the theory of electronic structure, in which the electron density distribution $\rho(\mathbf{r})$ rather than many-electron wave function plays a central role. In the spirit of Thomas-Fermi theory [19, 20], it is suggested that a knowledge of the ground state density of $\rho(\mathbf{r})$ for any electronic system uniquely determines the system.

3.1.1 Hohenberg-Kohn Formulation

The Hohenberg-Kohn [17] formulation of DFT can be explained by two theorems:

Theorem 1: The external potential is univocally determined by the electronic density, except for a trivial additive constant.

Since $\rho(\mathbf{r})$ determines V($\mathbf{r}$), then it also determines the ground state wave function and gives us the full Hamiltonian for the electronic system. Hence $\rho(\mathbf{r})$ determines implicitly all properties derivable from H through the solution of the time-dependent Schrodinger equation.

Theorem 2: (Variational Principle) The minimal principle can be formulated in terms trial charge densities, instead of trial wavefunctions.

The ground state energy E could be obtained by solving the Schrodinger equation directly or from the Rayleigh-Ritz minimal principle:

$$E = min \frac{\langle \widetilde{\Psi}|H|\widetilde{\Psi}\rangle}{\langle \widetilde{\Psi}|\widetilde{\Psi}\rangle} \tag{3.1}$$

Using $\widetilde{\rho}(\mathbf{r})$ instead of $\widetilde{\Psi}(\mathbf{r})$ was first presented in Hohenberg and Kohn. For a non-degenerate ground state, the minimum is attained when $\widetilde{\rho}(\mathbf{r})$ is the ground state density. And energy is given by the equation:

$$E_V[\widetilde{\rho}] = F[\widetilde{\rho}] + \int \widetilde{\rho}(\mathbf{r})V(\mathbf{r})d\mathbf{r} \tag{3.2}$$

with

$$F[\widetilde{\rho}] = \langle \Psi[\widetilde{\rho}]|\widehat{T} + \widehat{U}|\Psi[\widetilde{\rho}]\rangle \tag{3.3}$$

and $F[\widetilde{\rho}]$ requires no explicit knowledge of V($\mathbf{r}$).

These two theorems form the basis of the DFT. The main remaining error is due to inadequate representation of kinetic energy and it will be cured by representing Kohn-Sham equations.

3.1.2 Kohn-Sham Equations

There is a problem with the expression of the kinetic energy in terms of the electronic density. The only expression used until now is the one proposed by

Thomas-Fermi, which is local in the density so it does not reflect the short-ranged, non-local character of kinetic energy operator. In 1965, W. Kohn and L. Sham [18] proposed the idea of replacing the kinetic energy of the interacting electrons with that of an equivalent non-interacting system. With this assumption density can be written as

$$\rho(\mathbf{r}) = \sum_{s=1}^{2} \sum_{i=1}^{N_s} |\varphi_{i,s}(\mathbf{r})|^2 \tag{3.4}$$

$$T[\rho] = \sum_{s=1}^{2} \sum_{i=1}^{N_s} \langle \varphi_{i,s}| - \frac{\nabla^2}{2} |\varphi_{i,s}\rangle \tag{3.5}$$

where $\varphi_{i,s}$'s are the single particle orbitals which are also the lowest order eigenfunctions of Hamiltonian non-interacting system

$$\{-\frac{\nabla^2}{2} + v(\mathbf{r})\}\varphi_{i,s}(\mathbf{r}) = \epsilon_{i,s}\varphi_{i,s}(\mathbf{r}) \tag{3.6}$$

Using new form $T[\rho]$ density functional takes the form

$$F[\rho] = T[\rho] + \frac{1}{2}\int\int \frac{\rho(\mathbf{r})\rho(\mathbf{r}')}{|\mathbf{r}-\mathbf{r}'|} d\mathbf{r}d\mathbf{r}' + E_{XC}[\rho] \tag{3.7}$$

where this equation defines the exchange and correlation energy as a functional of the density. Using this functional in 3.2, we finally obtain the total energy functional which is known as Kohn-Sham functional [18]

$$E_{KS}[\rho] = T[\rho] + \int \rho(\mathbf{r})v(\mathbf{r})d\mathbf{r} + \frac{1}{2}\int\int \frac{\rho(\mathbf{r})\rho(\mathbf{r}')}{|\mathbf{r}-\mathbf{r}'|} d\mathbf{r}d\mathbf{r}' + E_{XC}[\rho] \tag{3.8}$$

in this way we have expressed the density functional in terms KS orbitals which minimize the kinetic energy under the fixed density constraint. In principle these orbitals are a mathematical object constructed in order to render the problem more tractable, and do not have a sense by themselves. The solution of KS equations has to be obtained by an iterative procedure, in the same way of Hartree [21] and Hartree-Fock [22, 23] equations.

3.2 Exchange and Correlation

3.2.1 Local Density Approximation (LDA)

The local density approximation [24] has been the most widely used approximation to handle exchange correlation energy. Its philosophy was already present in Thomas-Fermi theory but it was first presented by Kohn-Sham. The main idea of LDA is to consider the general inhomogeneous electronic systems as locally homogeneous and then use the exchange correlation corresponding to the homogeneous electron gas.

LDA favors more homogeneous systems. It over-binds molecules and solids but the chemical trends are usually correct.

3.2.2 Generalized Gradient Approximation (GGA)

Once the extent of the approximations involved in the LDA has been understood, one can start constructing better approximations. The most popular approach is to introduce semi-locally the inhomogeneties of the density, by expanding $E_{XC}[\rho]$ as a series in terms of the density and its gradients. This approximation is known as GGA [25] and its basic idea is to express the exchange-correlation energy in the following form:

$$E_{XC}[\rho] = \int \rho(\mathbf{r})\epsilon_{XC}[\rho(\mathbf{r})]d\mathbf{r} + \int F_{XC}[\rho(\mathbf{r}, \nabla\rho(\mathbf{r}))]d\mathbf{r} \tag{3.9}$$

where the function F_{XC} is asked to satisfy the formal conditions.

GGA approximation improves binding energies, atomic energies, bond lengths and bond angles when compared the ones obtained by LDA.

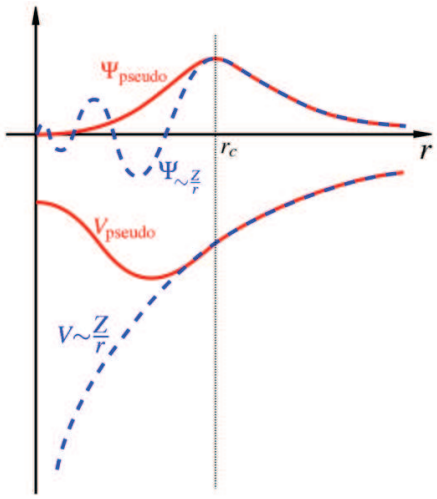

Figure 3.1: Illustration of all-electron (dashed lines) and pseudoelectron (solid lines) potentials and their corresponding wave functions.

3.3 Pseudopotential Approximation

It is well-known that most physical properties of solids are dependent on the valence electrons to a much greater extent than on the core electrons. The pseudoptential approximation utilizes this idea by replacing the core electrons and the strong ionic potential by a weaker pseudopotential that acts on a set of pseudo wave functions rather than the true valence wave functions. An ionic potential, its pseudopotential and corresponding wave functions are illustrated in Fig. 3.1.

Chapter 4

Si_nGe_n Nanowire Superlattices

4.1 Introduction

Planar superlattices have been fabricated either through periodic junction of alternating semiconductor layers with different band gaps or through repeating compositional modulation. Electrons in parallel layers show two-dimensional (2D) free electron-like behavior and have quantization different from those 3D bulk semiconductors. Minibands in the momentum space in the direction perpendicular to the layers and periodically varying band gap in the direct space have attributed unusual electronic functions for novel devices. These devices are field effect transistors, photodetectors, light emitting diodes (LEDs) and quantum cascade lasers etc.

Recently, new growth techniques have enabled also the synthesis of one-dimensional (1D) nanowire superlattices (NWSLs). NWSLs from group III-V and group IV elements have been synthesized successfully. InAs/InP superlattices [14] with atomically perfect interfaces and with periods of several nanometers could be realized using techniques, such as molecular beam epitaxy and nanocluster catalyst. Furthermore, compositionally modulated superlattices of GaAs/GaP have been synthesized by laser-assisted catalytic growth technique [9] again with atomically perfect interfaces and with the component layers ranging from 2 to 21.

It is proposed that these NWSL's can offer potential applications in nanoelectronics such as optical nanobar codes, 1D waveguides and polarized nanoscale LEDs. Longitudinal Si/Si-Ge NWSL with nanowire diameter ranging from 50 to 300 nm have been also synthesized using laser ablation growth technique.[12] Structural parameters such as nanowire diameter, Ge concentration and the modulation period in the Si/Si-Ge superlattices can be controlled easily by adjusting the reaction conditions. Technological applications such as LEDs and thermoelectric devices have been suggested. In addition to the longitudinal (axial) nanowire superlattices, coaxial core-shell and core-multishell nanowire heterostructures have attracted interest recently. Crystalline Si/Ge and Ge/Si core-shell structures have been experimentally synthesized by Lauhon *et al.*[26] Most of works involved in 1D superlattices especially concern the experimental synthesis and characterization of coaxial nanowire heterostructures.

Theoretically, only a few works investigated core-shell and longitudinal NWSL's.[27, 28, 29, 30] Kagimura *et al.* [28] reported an *ab initio* study of the electronic properties of Si and Ge nanowires, Si/Ge heterostructures with one surface dangling bond state per unit cell. They concluded that surface dangling bond level observed in the band gap of nanowires and nanowire heterostructures can be used as reference level to estimate band lineups in these systems. Using one-band effective mass theory, a criterion has been developed for the occurrence of longitudinal barrier height.[29] It has been argued that radial confinement reduces the actual barrier height in modulated nanowire superlattices. Zypman [30] used the Hubbard model to get the energy spectrum of one-dimensional systems and applied their results to various model systems like nanowire tunnelling diodes and Si/Ge superlattice nanowires to interpret the scanning tunnelling spectroscopy measurements. Earlier formation of multiple quantum well structure and resulting confined states on hydrogenated or radially deformed carbon nanotubes have been also reported.[31]

In this thesis, we have investigated mechanical properties, atomic and electronic structures of bare and hydrogenated Si_nGe_n nanowire superlattices using first-principles plane wave method. NWSL's are constructed from alternating Si and Ge nanowire segments (zones), both have same orientation and similar atomic

structure. These segments are joined pseudomorphically and formed a sharp interface. We found that even a small diameter hydrogenated Si_nGe_n NWSL's form multiple quantum well structures where conduction and valence band electrons are confined. Our study indicates that the band lineup and resulting electronic structure depend on the length and cross section geometry of the constituent Si_n and Ge_n nanowires.

4.2 Method of calculations

We have performed first-principles plane wave calculations [32, 33] within DFT [34] using ultra-soft pseudopotentials.[33, 35] The exchange correlation potential has been approximated by generalized gradient approximation GGA using PW91 functional.[36] For partial occupancies we use the Methfessel-Paxton smearing method.[37] The adopted smearing width is 0.1 eV for the atomic relaxation and 0.02 for the accurate band structure analysis and density of state calculations. All structures have been treated within a supercell geometry using the periodic boundary conditions. The lattice parameters of the tetragonal supercell are a_{sc}, b_{sc} and c_{sc}. We took $a_{sc} = b_{sc}$=27 Å for NWSL having the largest diameter ($\sim$ 1.8 nm), but $a_{sc} = b_{sc}$=22 Å for one having the smallest diameter ($\sim$ 1.2 nm) considered in this paper. These values allowed minimum distance ranging from $\sim$ 11 Å to 14 Å between two atoms in different adjacent cells, so that their coupling is hindered significantly. We took c_{sc} equal to the lattice constant c of the nanowires and NWSLs under consideration. In the self-consistent potential and total energy calculations the Brillouin zone (BZ) is sampled in the **k**-space within Monkhorst-Pack scheme [38] by (1x1x9) mesh points for single unit cell and for example (1x1x5) mesh points for double cells. A plane-wave basis set with kinetic energy up to 250 eV has been used. All atomic positions and lattice constant $c_{sc} = c$ are optimized by using the conjugate gradient method where total energy and atomic forces are minimized. The criterion of convergence for energy is chosen as 10^{-5} eV between two ionic steps, and the maximum force allowed on each atom is 0.05 eV/Å.

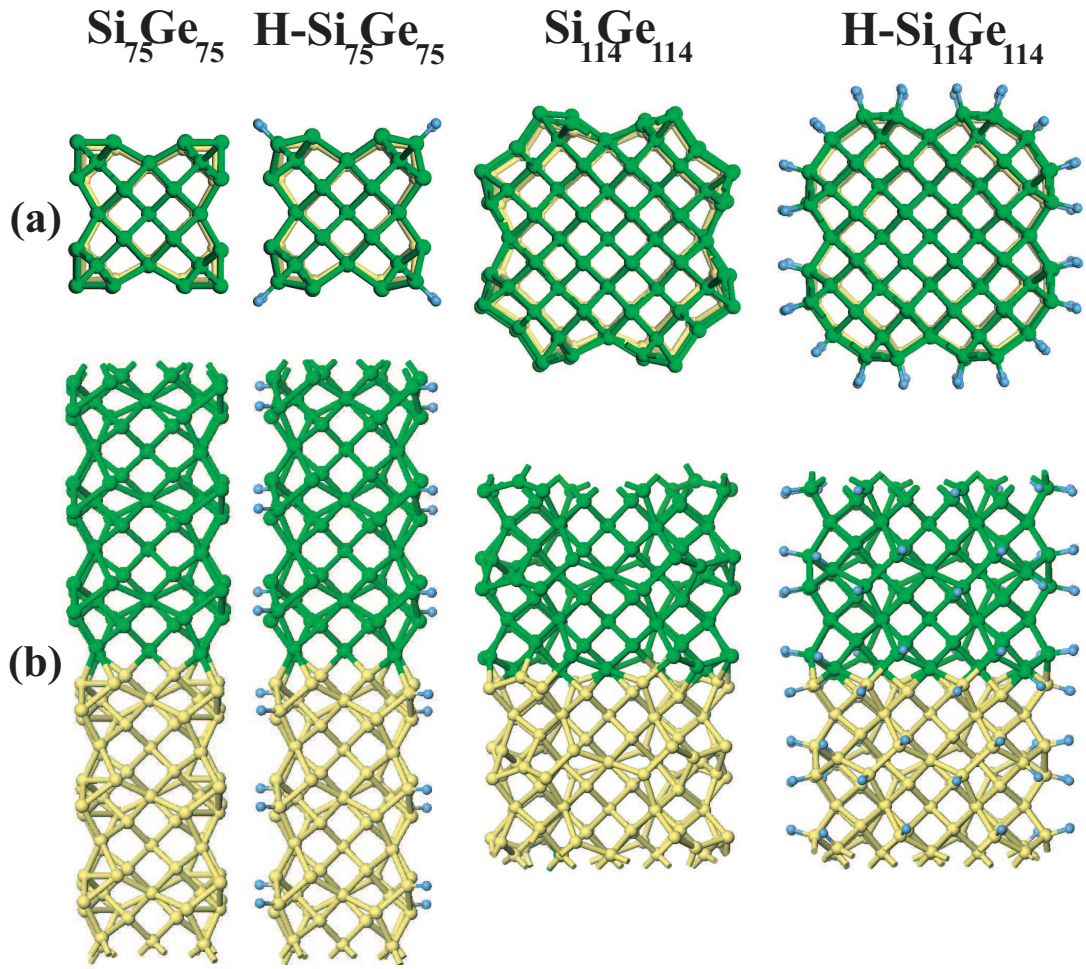

Figure 4.1: Optimized atomic structure of bare and hydrogenated Si_nGe_n nanowire superlattices for n=75 and 114. a) Top view; b) Side view. Small-gray, large-light and large-dark balls correspond to the hydrogen, silicon and germanium atoms respectively.

4.3 Bare and Hydrogenated Nanowires and Nanowire Superlattices

In this study we considered bare and hydrogen passivated longitudinal Si_nGe_n nanowire superlattices and also bare and hydrogen passivated Si and Ge nanowires as constituent structures. Bare Si and Ge nanowires are oriented along [001] direction of the parent diamond crystal and have normally N atoms in their primitive unit cell with lattice constant c along the nanowire (or z-) axis. We took N=25 and N=57 as two special prototypes. We designate them as SiNW(n) [GeNW(n)] or shortly Si_n (Ge_n) with n=sN, s being an integer number. Si_n and Si_N (Ge_n and Ge_N) indicates the same nanowire, except that the unit cell of the former one includes s primitive cell in direct space with *1/s* times reduced BZ in the momentum space. In our simulations bare Si_n (Ge_n) nanowires are first cut from the bulk crystal with ideal structural parameters. Subsequently ideal bare nanowires are relaxed to optimize their structure and lattice constant. Si (Ge) atoms near the core of relaxed nanowire has tetrahedral coordination. To obtain H-passivated Si_n or Ge_n nanowires (designated as H-SiNW(n) or H-GeNW(n), shortly as H-Si_n or H-Ge_n) the dangling bonds at the surface are saturated by H atoms and whole structure is re-optimized. Our study indicates that the atomic and electronic structure of H-Si_n and H-Ge_n may depend on whether hydrogen passivation and subsequent optimization are achieved on ideal or optimized bare Si_n and Ge_n nanowires. The present sequence of structure optimization mimics the actual growth of hydrogen passivated nanowires.

A Si_nGe_n has n=sN Si atoms at one side and n=sN Ge atoms at the other side of NWSL unit cell. These atoms have tetrahedral coordination as if they are part of a SiGe heterostructure and hence at the interface Si atoms are bonded to Ge atoms pseudomorphically and make atomically flat interface. We note that pseudomorphic growth can sustain for small diameters; but misfit dislocations may be generated at the interface of large diameter (or large N) Si_nGe_n superlattice. Atomic positions and lattice constant are relaxed to obtain optimized structure. H-Si_nGe_n follow the same sequence of construction as H-Si_n or H-Ge_n. Optimized lattice constants of bare Si_nGe_n nanowire superlattice for n=25, 50

and 75 are found to have c=10.9 Å, 21.8 Å and 32.7 Å, respectively. Upon hydrogenation these lattice constants change to c=11.2 Å, 22.3 Å and 33.5 Å, respectively. Lattice constants of bare and hydrogenated Si_nGe_n, n=57 and 114 are almost identical and are c=11.1 Å and 22.2 Å, respectively. Fig.4.1 shows the atomic structure of bare and hydrogen passivated Si_nGe_n for n=75 and 114. These NWSLs are reminiscent of Si_nGe_n (001) planar superlattice which were fabricated by molecular beam epitaxy by growing first n Si (001) plane and then n Ge (001) plane, and eventually by repeating this Si_nGe_n (001) unit periodically. While the Si_nGe_n (001) superlattice has 2D periodicity in (001) layers, NWSLs under study here have finite cross section and hence 2D periodicity is absent. Electrons are bound to NWSL in radial (lateral) direction, but propagate as 1D Bloch states along the superlattice axis (in longitudinal direction).

Interatomic distance distribution of $Si_{75}Ge_{75}$ and H-$Si_{75}Ge_{75}$ NWSLs are compared with parent Si and Ge nanowires in Fig.4.2. In the same figure we also show the interatomic distance distribution of bare and hydrogenated $Si_{114}Ge_{114}$ NWSL. At the surface, optimized atomic structures of Si_n and Ge_n deviate considerably from the ideal structure of Si_n and Ge_n. For example, one can deduce quadrangles of atoms at the surface. Normally, NWSLs consist of hexagonal and pentagonal rings, where one can distinguish bond lengths in different categories. The interatomic distance distribution of Si_nGe_n is reminiscent of the sum of those of Si_{2n} and Ge_{2n} except some changes originated from the interface between Si and Ge segments of supercell. While bulk optimized Si-Si and Ge-Ge bond lengths are d=2.36 Å, and 2.50 Å, respectively, the Si-Ge bond at the interface ranges between 2.35 Å and 2.52 Å for bare $Si_{228}Ge_{228}$ (between 2.37 Å and 2.49 Å for H-$Si_{228}Ge_{228}$). Nevertheless, the distribution exhibit several peaks corresponding to the deviations from the bulk geometry at the surface. As the cross section or N increases the effect of the surface decreases and the distribution of interatomic distances becomes more bulk-like.

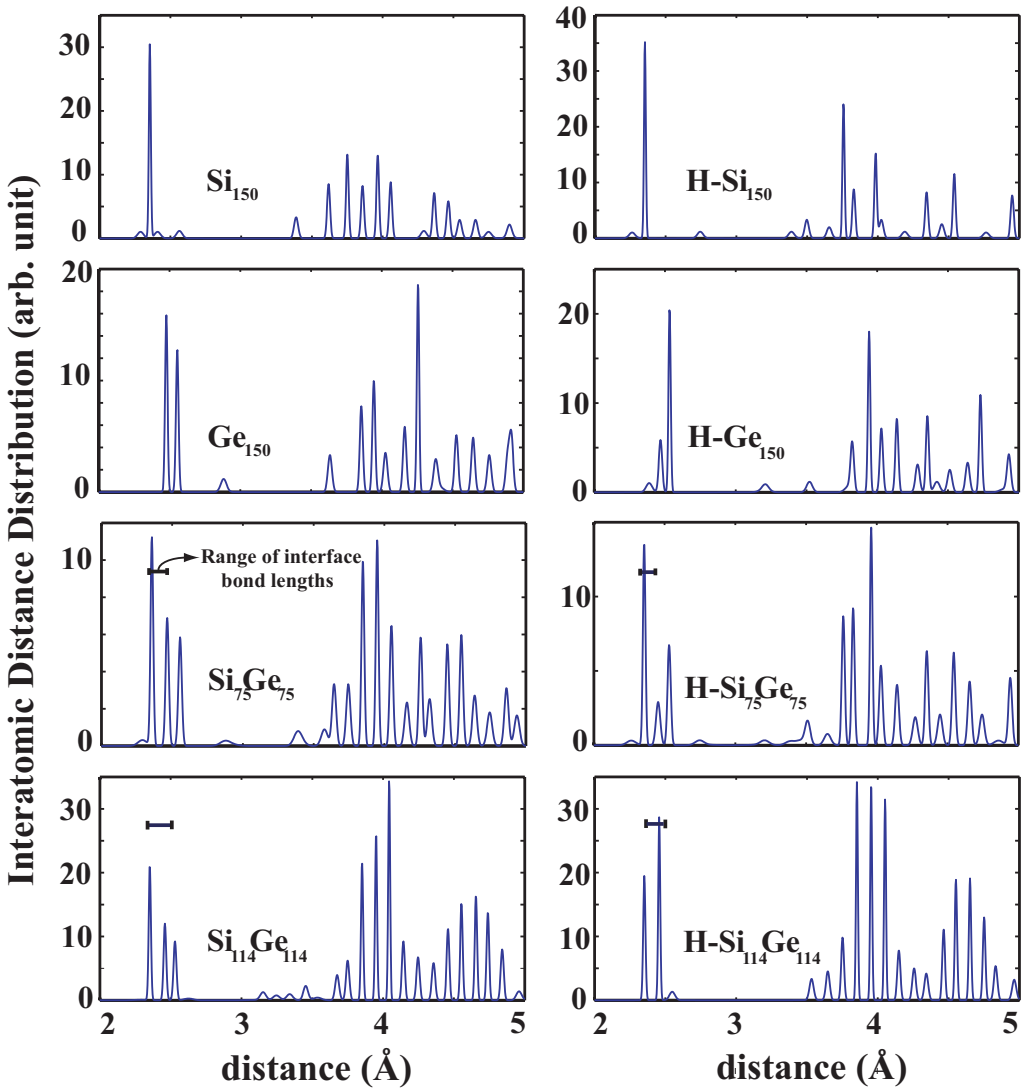

Figure 4.2: Interatomic distance distribution of optimized bare and hydrogenated Si_{2n}, Ge_{2n} and Si_nGe_n for n=75 up to fourth nearest neighbor. The similar distribution for $Si_{114}Ge_{114}$ and H-$Si_{114}Ge_{114}$ are also shown. The Si-H (Ge-H) bond lengths being in the range of ($\sim$ 1.5 Å) are not shown.

4.4 Mechanical properties

The stability and elasto-mechanical properties of Si_nGe_n and H-Si_nGe_n NWSLs are crucial for their possible use in nanoelectronics. In the present study the maximum diameter of nanowire we treated is $\sim$ 1.8 nm. The diameter of hydrogenated $Si_{25}Ge_{25}$ NWSL is even smaller ($\sim$ 1.4 nm). For such small diameter nanowires or NWSL's, there are ambiguities in determining the area of cross section. Moreover, the surface to volume ratio is rather high and hence makes the cross section nonuniform. In view of these, the calculation of Young's modulus may not be appropriate. Here we rather considered the force (spring) constants of nanowires and NWSLs under a strain in the harmonic region. To this end we calculated the second derivative of the total energy (per unit cell) with respect to the lattice constant c (*i.e.* κ=d^2E_T/dc^2) or to the strain, ϵ=$\Delta c/c$ (*i.e.* κ'=$d^2E_T/d\epsilon^2$). The values calculated for nanowires and NWSLs treated in our paper are given in Table 4.1.

Like bulk crystals, Si_n nanowires are stiffer than Ge_n nanowires. This implies that the lattice mismatch between Si and Ge nanowires in NWSL is accommodated mainly by the Ge zone. For both nanowires and NWSL, κ increases with increasing cross section. For example κ of Si_{25} is almost the half of κ of Si_{57}. Note that $\kappa(Si_{50}) \simeq \kappa(Si_{25})/2$. As for, κ of $Si_{25}Ge_{25}$ NWSL calculated from first principles is 2.18 eV/Å. This value can be estimated in terms of two springs connected in series, namely $\kappa^{-1}(Si_{25}Ge_{25}) \simeq \kappa^{-1}(Si_{25})+\kappa^{-1}(Ge_{25})$ to be $\kappa(Si_{25}Ge_{25})$ $\simeq$ 2.08 eV/Å. We, therefore, conclude that as long as the geometry and size of the cross section remained to be similar, classical Hook's law continues to be approximately valid even for nanostructures. Upon hydrogenation both nanowires as well as NWSLs studied here become stiffer. The spring constant of $Si_{57}Ge_{57}$ is twice that of $Si_{114}Ge_{114}$, because the latter NWSL has twice the length of the former. We also calculated the ratio of the strain of the Ge-zone to that of Si-zone of $Si_{75}Ge_{75}$ under tensile stress, *i.e.* ϵ (Ge)/ϵ (Si) to be $\sim$ 2.5. These calculations have been performed by minimizing the total energy under a preset uniaxial strain in the elastic range. The strain on Ge and Si-zone calculated are determined after full relaxation. The ratio found is reduced to $\sim$ 1.25 for $Si_{114}Ge_{114}$. In compliance

Table 4.1: Equilibrium values of lattice parameter c are given in units of Å. Force constant κ (as defined in the text), in units of eV/Å, is calculated by using both VASP result and Hook's law. Percentage difference in between force constant values calculated from VASP result and Hook's law is given within parenthesis in order to check whether classical Hook's law is still valid in nanoscale. Also force constant κ' (as defined in the text) is presented in units of eV.

Structure	c_o	κ	Hook's Law	κ'
Si_{25}	5.32	5.68		161
Ge_{25}	5.57	3.28		102
$Si_{25}Ge_{25}$	10.90	2.18	2.08	259
$Si_{50}Ge_{50}$	21.75	0.92	1.04	437
$Si_{75}Ge_{75}$	32.70	0.62	0.69	663
Si_{57}	5.43	11.22		327
Ge_{57}	5.65	7.49		239
$Si_{57}Ge_{57}$	11.07	4.24	4.49	522
$Si_{114}Ge_{114}$	22.15	2.10	2.25	1035
H-Si_{25}	5.45	8.56		254
H-Ge_{25}	5.73	5.98		196
H-$Si_{25}Ge_{25}$	11.17	3.48	3.52	436
H-$Si_{50}Ge_{50}$	22.30	1.70	1.76	845
H-$Si_{75}Ge_{75}$	33.50	1.14	1.17	1279
H-Si_{57}	5.39	13.57		394
H-Ge_{57}	5.68	11.09		358
H-$Si_{57}Ge_{57}$	11.05	6.13	6.10	755
H-$Si_{114}Ge_{114}$	22.08	3.33	3.05	1626

with the κ values in Table 4.1, this result indicates that in a Si_nGe_n NWSL Ge zone elongates more than Si-zone. Using empirical potential, Menon *et al.* [39] were able to calculate the Young's modulus and bending stiffness of tetrahedral and cage-like Si nanowire of ~ 4 nm diameter, and found values comparable with bulk values.

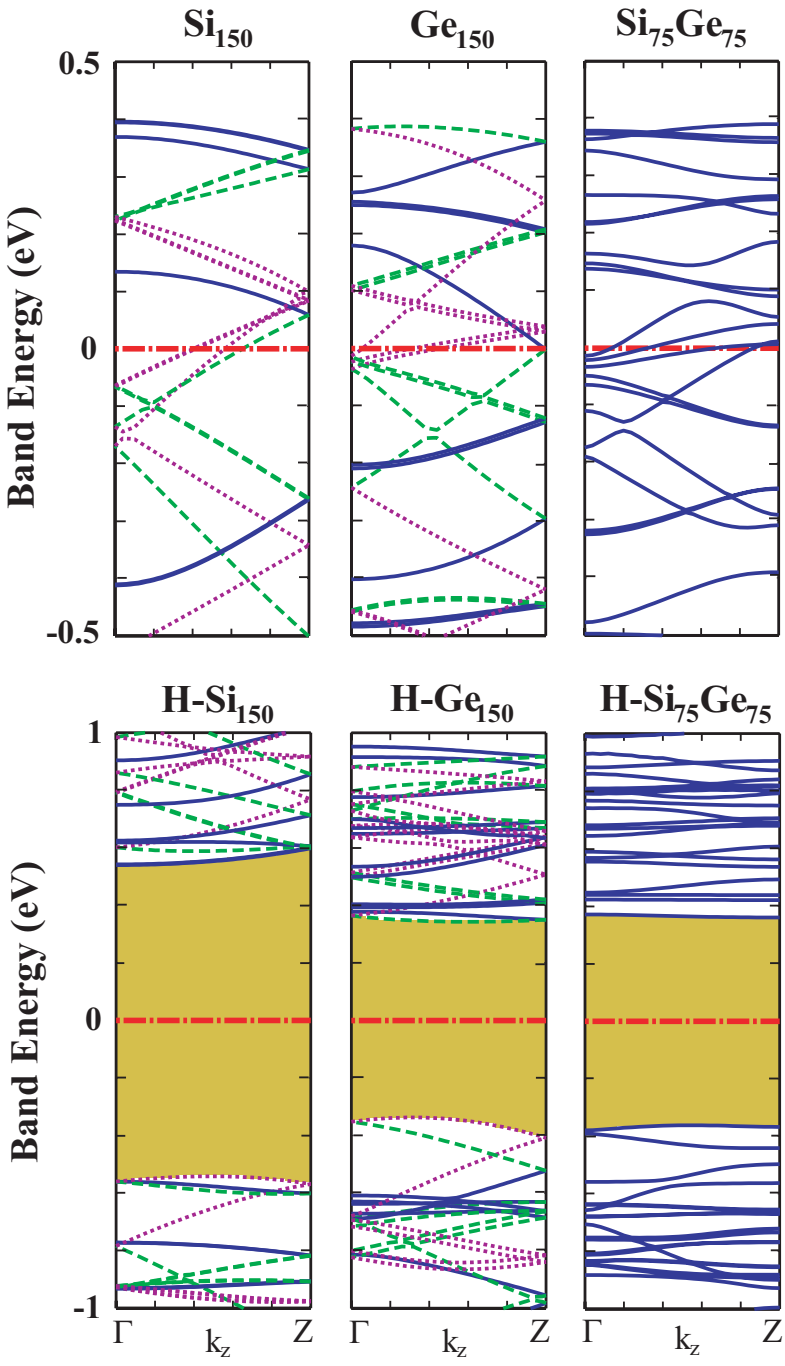

Figure 4.3: Energy band structures of optimized bare and hydrogenated Si_{2n}, Ge_{2n} nanowires and Si_nGe_n nanowire superlattices for n=75. Zero of energy is taken at the Fermi level. Band gaps are shown by shaded zones. Dashed and dotted lines (minibands) are obtained by folding of Si_{50} (also H-Si_{50}) and Ge_{50} (also H-Ge_{50}) bands.

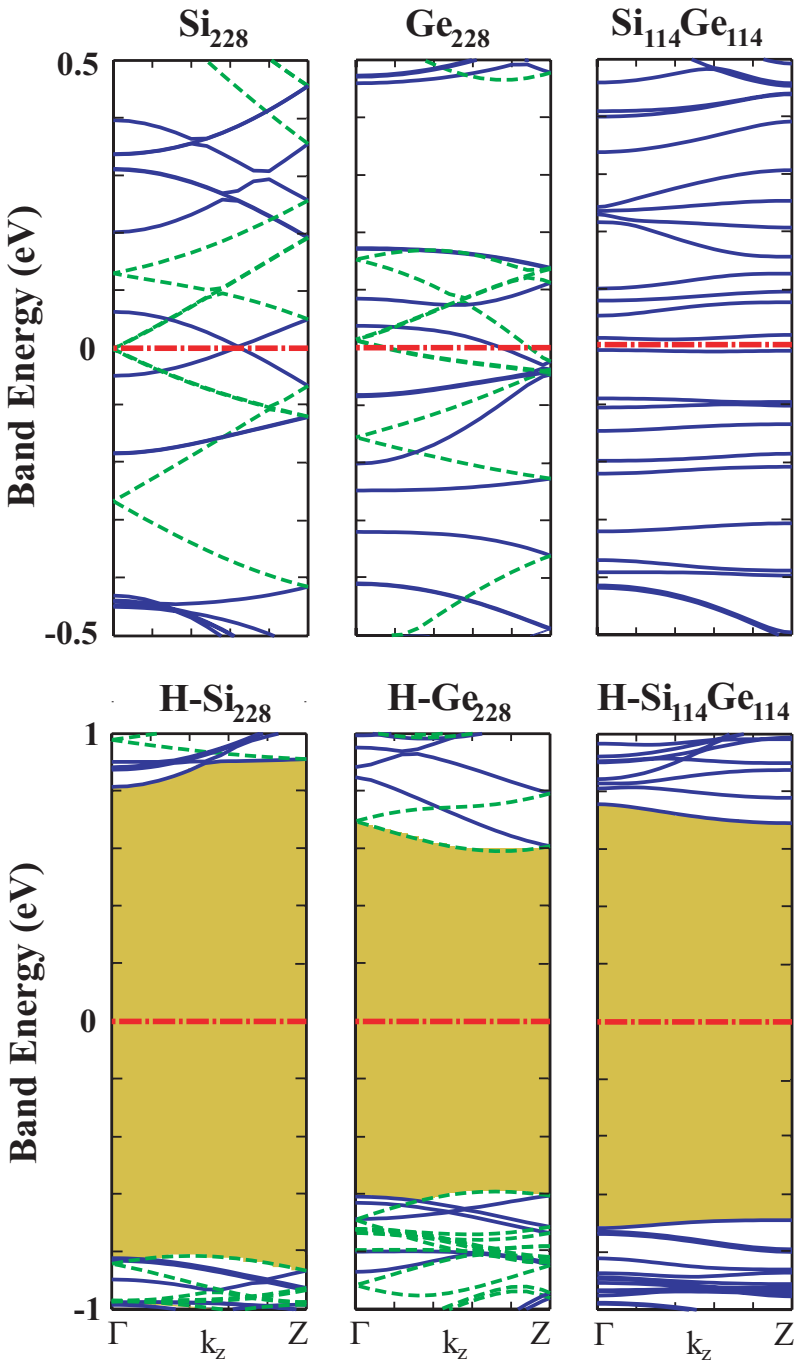

Figure 4.4: Energy band structures of optimized bare and hydrogenated Si_{2n}, Ge_{2n} nanowires and Si_nGe_n nanowire superlattices for n=114. Zero of energy is taken at the Fermi level. Dashed and dotted lines are obtained by folding of Si_{57} (also H-Si_{57}) and Ge_{57} (also H-Ge_{57}) bands.

4.5 Electronic Properties

The band structures of optimized bare and hydrogenated Si_nGe_n are given in Fig.4.3 and Fig.4.4 for n=75 and 114, respectively. In the same figures the band structures of bare and hydrogenated Si_{2n} and Ge_{2n} constituent nanowires are presented for the sake of comparison. Si_N (N=25 and 57) and hence any Si_{2n} (n=sN) nanowires are metallic due to the surface dangling bonds. Similarly Ge_N (N=25 and 57) and hence any Ge_{2n} are metallic. Upon passivation of dangling bonds, these metallic nanowires become semiconductor. For example, H-Si_{150} and H-Ge_{150} nanowires have indirect band gaps, E_g=1.1 eV and 0.7 eV, respectively. Normally, the band gap of a H-Si_n is inversely proportional to its diameter, if the corresponding ideal nanowire cut from the bulk crystal were directly passivated with H before the structural optimization. Also the band gap is affected by the cross section geometry for small N. For large N, the variation of E_g with N is more uniform.

Like Si_{150} and Ge_{150}, $Si_{75}Ge_{75}$ is metallic. The ideal equilibrium ballistic conductance of Si_{150}, Ge_{150} nanowires and $Si_{75}Ge_{75}$ NWSL is revealed to be $6e^2/h$, $10e^2/h$ and $8e^2/h$, respectively. Since H-Si_{150} and H-Ge_{150} are semiconductors, H-$Si_{75}Ge_{75}$ NWSL is also semiconductor: Its band gap is 0.7 eV and close to the band gap of H-Ge_{150}. H-$Si_{114}Ge_{114}$ has a direct band gap of 1.4 eV. Again it is smaller than the band gap of H-Si_{228}, but closer to that of H-Ge_{228}.

In Fig.4.5 we examine how the electronic energy bands of nanowire superlattices evolve with the lattice constant c or s. In the case of N=25, bare Si_nGe_n nanowire superlattices are metallic for all n (n=25, 50 or s=1, 2 and 3). As s increases additional minibands occur and they become flatter. As for H-Si_nGe_n's, they are all semiconductor for n=25, 50 and 75. As n increases all bands including lowest conduction and highest valence band become flatter with the formation of minibands. In this respect, the band gap becomes more uniform as s increases. Similar behaviors are displayed also for H-Si_nGe_n with n=57 and 114 (see Fig.4.4). Unexpectedly, bare Si_nGe_n's are semiconducting for n=57 and 114. The band gap decreases from 0.27 eV to 0.02 eV as s increases from 1 to 2. Isosurface charge densities of these states near the band gap edges found that they are confined in

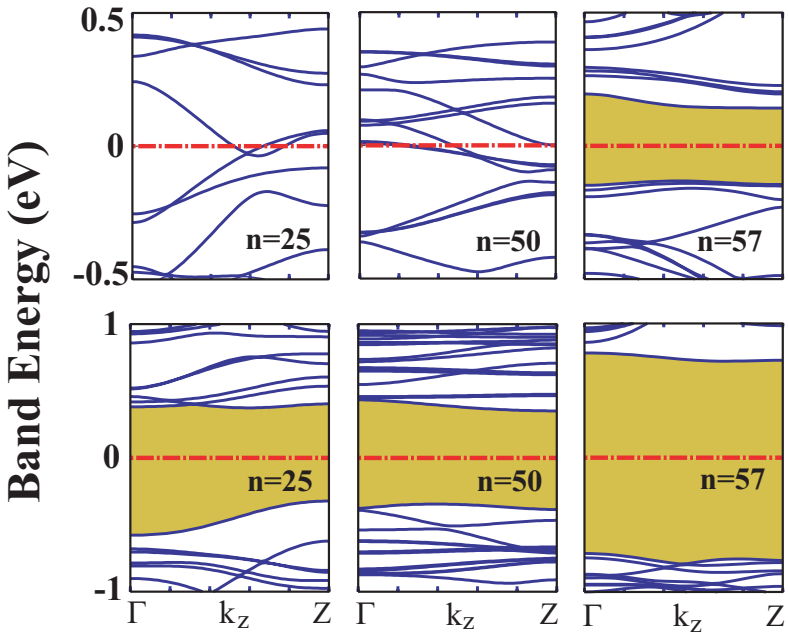

Figure 4.5: Energy band structure of bare and hydrogenated Si_nGe_n nanowire superlattices for n=25, 50 and 57.

one of the zones. It is concluded that opening of the band gap originates from the mismatch of surface dangling bond states in Si and Ge zones.

It should be noted that the band gap is underestimated by the GGA calculations used in the present study. GW corrections performed recently [40] for H-Si_n in different orientation is in the range of 0.5-0.6 eV for large diameters. In view of the fact that Ge bulk is predicted as metal by GGA calculation, GW correction for H-Ge_n nanowires is expected to be in the same range as that for H-Si_n. Under this circumstances a scissor operation (namely increasing the band gap of corresponding Si_nGe_n by the same amount 0.5-0.6 eV) may yield the actual band gap. In summary, the band gaps of H-Si_nGe_n predicted by GGA calculation are underestimated, and actual bands are expected to be 0.5-0.6 eV larger.

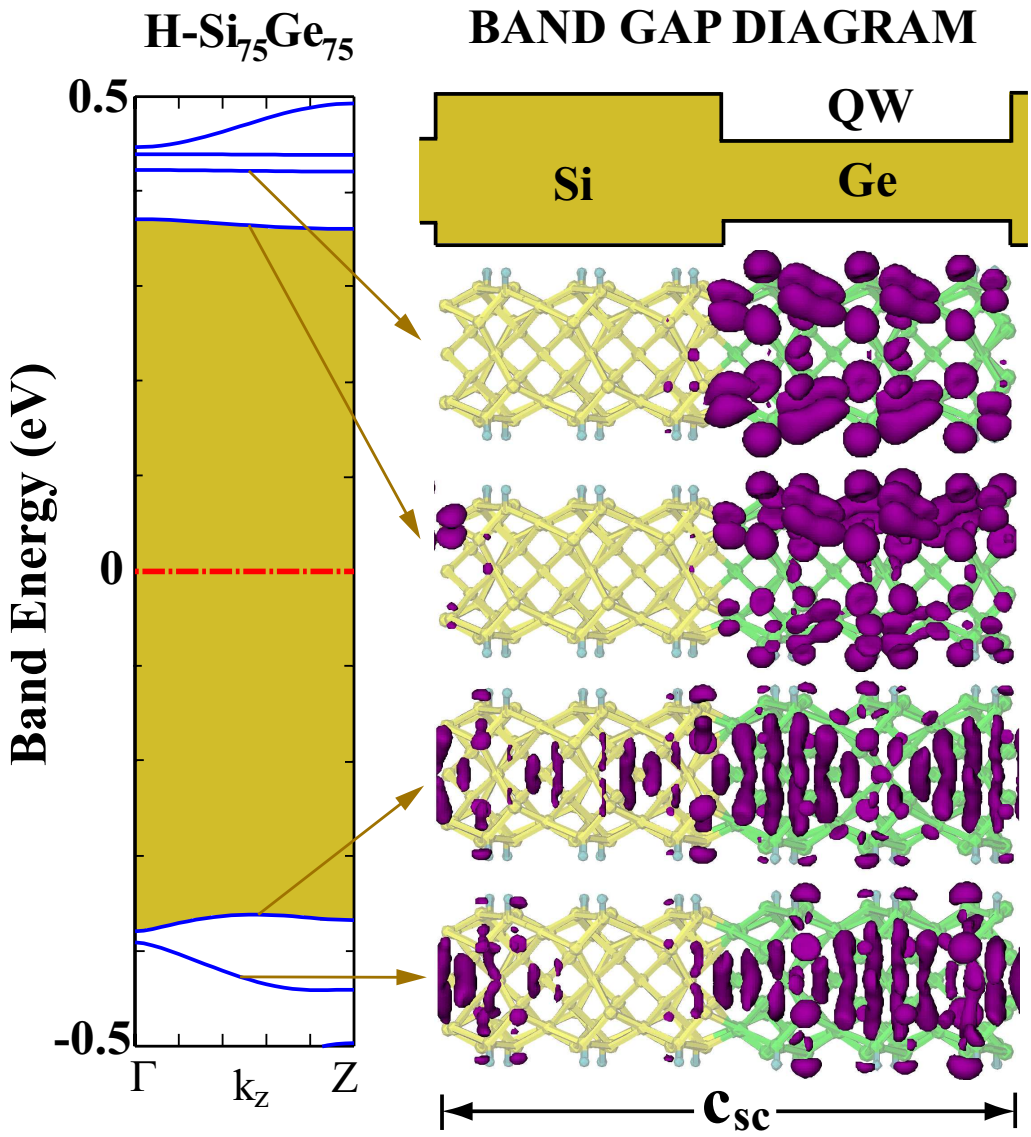

Figure 4.6: Schematic description of energy band diagram in the unit cell (on the right and upper side), band structure in momentum space (on the left side) and isosurface charge density of states of H-$Si_{75}Ge_{75}$ NWSL at the band edges.

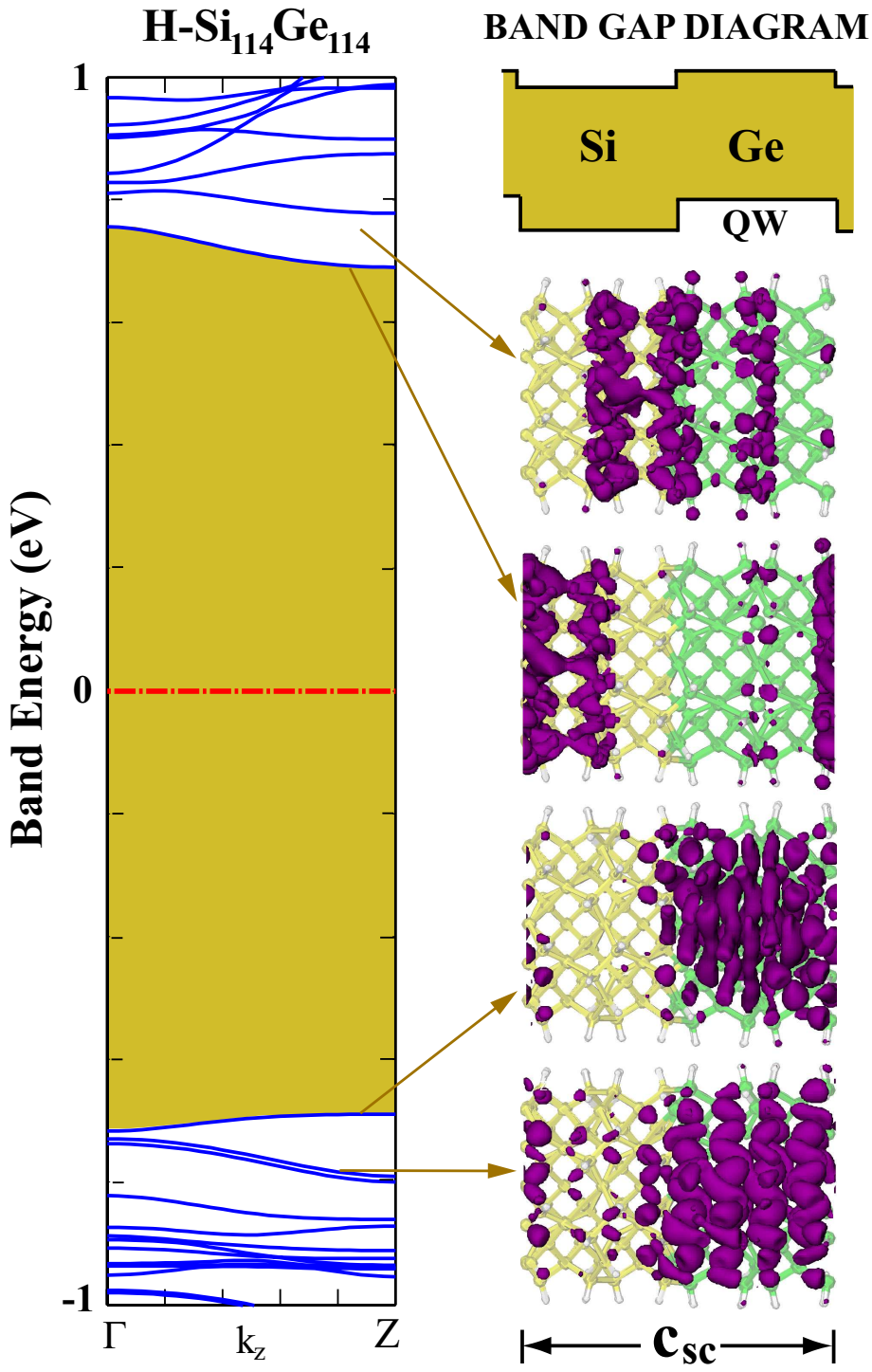

Figure 4.7: Schematic description of energy band diagram in the unit cell (on the right and upper side),band structure in the momentum space (on the left side) isosurface charge density of states of H-$Si_{114}Ge_{114}$ NWSL at the band edges.

4.6 Confined states

The results discussed in the previous section reveals that Si_n and Ge_n nanowires making a Si/Ge heterojunction in the supercell have band gaps of different width. Upon a pseudomorphic junction the bands and hence band gaps corresponding to Si and Ge zones are aligned. Combination of two features, namely Si and Ge zones having different band gaps and band-lineup result in band discontinuities and hence band-offsets. The conduction and valence band edges of different zones (Si-zone or Ge-zone) in the nanowire superlattice will have different energies. Under these circumstances, the diagram of the conduction band edge along the axis of NWSL will display a multiple quantum well structure with the periodicity of c_{sc} like a Kronig-Penny model. Electrons in the well region of a zone should decay in the adjacent zones having higher conduction band edge, since their energy will fall into the band gap of this barrier zone. As a result, the states of these confined (or localized) electrons are propagating in the well, but decaying in the barrier. Usually, confined electrons have low group velocity. They may become more localized if the barrier is high and the width of barrier is large. If the confinement (or localization) is complete, electrons in adjacent levels do not interact and the associated band $E_n(k_z)$ becomes flat. Accordingly, such a state has $\int_{well} \Psi_c^* \Psi_c \overrightarrow{dr} \gg \int_{barrier} \Psi_c^* \Psi_c \overrightarrow{dr}$. This is known as Mott localization. Similar arguments are valid for the hole states if the energies of valence band edges of both zones are different.

In the past, the reference energies in determining band-offsets of 2D superlattices have been actively studied both experimentally and theoretically. Energy diagram of conduction and valence band edges are then used as effective potential forming a multiple quantum well structure.[41] The states of conduction band electrons and holes of valence band were treated using Effective Mass Theory (EMT). These states are free electron-like 2D bands in the planes and Bloch states forming minibands perpendicular to the planes. The conditions are, however, different in NWSLs. First of all, EMT may not be applicable directly in the present case, in particular for NWSLs with small diameter. Secondly, the reference energy level determined for planar superlattices may not be appropriate.

Recently, Kagimura *et al.* [28] proposed surface dangling bond states as reference level for Si/Ge core-shell superlattices. Under estimation of band gaps by DFT GGA calculation may hinder the accurate determination of band-lineups. Voon and Willatzen [29] draw attention to the lateral confinement of states in NWSL's. Using one-band EMT and by solving Ben Daniel-Duke [42] equation they found that the effective barrier is lowered due to the coupling between radial and longitudinal confinement. In particular, they predicted, that the effective barrier and hence confinement disappears below a critical radius of $\sim$ 5 nm. In the present study, the maximum radius of NWSL was $\sim$ 0.9 Å which is much lower than the critical radius set for GaAs/AlGaAs NWSLs.[29]

In the present study we examined whether some of states can be longitudinally confined, by performing an extensive analysis of charge densities of superlattice bands calculated by first-principle methods. The formation of periodic quantum well structure is schematically described in Fig.4.6. We expect that the values of band gaps in the H-Si and H-Ge zones in a unit cell of the H-$Si_{75}Ge_{75}$ cannot deviate significantly from the values calculated for periodic H-Si_{25} and H-Ge_{25} nanowires (namely, 1.1 eV and 0.7 eV, respectively). When the two zones are connected by an atomically flat interface, H-Ge zone can form a well between adjacent H-Si zones, since the band gap of the former zone is smaller and the energy of conduction band edge is lower relative to that of the latter zone. Upon normal band-lineup, H-Ge_{75} zone acts as a quantum well for both lowest conduction and highest valence band electrons. Band structure of H-$Si_{75}Ge_{75}$ with two lowest conduction and two highest valence minibands and their isosurface charge distribution in the superlattice unit cell are shown in Fig.4.6. The distribution of electronic charge density is confirming the above normal band-lineup. Both conduction band states are confined in the H-Ge_{75} zone, but they have very small weight in the H-Si_{75} zone. Similarly, states corresponding to two highest valence bands are also confined in the H-Ge_{75} zone. It should be noted that owing to the charge transfer between adjacent zone the form of the energy band diagram may change from the simple form given in Fig.4.6.

In Fig.4.7 we present similar analysis for H-$Si_{114}Ge_{114}$ NWSL. As compared to H-$Si_{75}Ge_{75}$, here H-Si and H-Ge zones are $\sim$ 5 $\mathring{A}$ shorter. However, there are more

minibands owing to larger number of Si and Ge atoms. The ways the highest valence band and the lowest conduction band states are confined in different zones suggest a staggered band line-up. Highest valence band states are confined in the H-Ge zone; but lowest conduction band states are confined in H-Si zone. States of 6^{th} and 7^{th} valence band (from the top) are propagating throughout the NWSL.

We believe that present *ab-initio* results revealing confined states for NWSLs with a radius as small as ~ 0.6 nm are not contradicting the conclusions obtained from one-band EMT model. We think EMT as applied in Ref. 7 has to be revised for small diameter NWSL. Moreover, the material parameters of GaAs/AlGaAs relevant for EMT by themselves are different from Si_nGe_n nanowire superlattices studied here. We also note that H-Si_nGe_n nanowire superlattice has 1D rodlike structure. There are several minibands in the 1D BZ. Number of minibands in a given energy interval increases with either increasing N (*i.e.* increasing diameter) or increasing s. A nanowire superlattice with a long unit cell having several Si or Ge atoms will have several (quasi continuous) minibands. States of H-Si_n or H-Ge_n zone of the same energy are more likely to match each other to construct a state that propagate throughout the NWSL. Otherwise, a superlattice of small radius with short unit cell have small number of bands. Then the states in different zones are less likely to match. A state, which cannot find a matching partner is confined to its zone. As a matter of fact, we were able to deduce confined states even in the barrier zone (H-Si) with energies higher than the conduction band edge.

Chapter 5

Size Modulated Si NWSL

Rod-like Si nanowires (SiNW) have been synthesized down to $\sim$ 1 nm diameter.[11] They are attractive one-dimensional (1D) materials because of the well-known silicon fabrication technology that make them directly usable on the Si-based chips. Even if unsaturated dangling bonds on the outer surface usually attribute a metallic character to SiNWs, they become insulator (or semiconductor) upon saturation of these dangling bonds by hydrogen atoms.[43] SiNWs display diversity of electronic properties depending on their diameter, as well as their orientation. In particular, the band gap of semiconductor SiNWs varies with their diameters. They can be used in various electronic, spintronic and optical applications, such as field effect transistors [44], light emitting diodes [45], lasers [46] and interconnects. The conductance of these semiconductor nanowires can be tuned easily by doping[47, 48] during the fabrication process or by applying a gate voltage. Recent studies have shown that 3d transition metal doped Si nanowires become half-metallic.[49]

5.1 Calculations and Results

This part of the thesis demonstrates that SiNWs of different diameters can form stable superlattices. The electronic band structure of the superlatice is different

from the constituent SiNWs and is modulated in real space leading to a multiple quantum structure and/or to a series of quantum dots. In these size induced quantum wells, specific states are confined. These results are obtained by performing first-principles plane wave calculations within Density Functional Theory (DFT)[34] using ultrasoft pseudopotentials.[35, 33] The exchange correlation potential has been approximated by GGA using PW91 functional.[36] All structures have been treated within supercell geometry using the periodic boundary conditions. A plane-wave basis set with kinetic energy cutoff of up to 250 eV has been used. In the self-consistent potential and total energy calculations the Brillouin zone is sampled in **k**-space within Monkhorst-Pack scheme[38] by (1×1×11) mesh points for the smallest structure. This sampling is scaled according to the size of superlattices. All atomic positions and lattice constants are optimized by using the conjugate gradient method where total energy and atomic forces are minimized. The convergence for energy is chosen as 10^{-5} eV between two steps, and the maximum force allowed on each atom is 0.02 eV Å.

Here Si nanowires (i.e. Si_{N_1} with diameter $\sim D_1$ and having N_1 Si atoms in the primitive unit cell) is first cut from the ideal bulk crystal along desired direction. Then in every alternating segment comprising l_1 unit cell the diameter D_1 is kept fixed, but in the adjacent segment comprising l_2 unit cell (each having N_2 Si atoms) the diameter is reduced to D_2. The latter part can be identified as the segment of Si_{N_2} nanowire. At the end, the segments of Si_{N_1} and Si_{N_2} have made a smooth junction and hence formed an ideal superlattice Si_N so that its diameter is modulated in real space. Note that $N \leq l_1N_1 + l_2N_2$, because some surface atoms attaching with a single bond to the surface were removed at the beginning. Subsequently we relaxed the atomic structure of bare and ideal Si_N. Upon relaxation, the dangling bonds on the surface are saturated by H atoms and Si_NH_M superlattice is further relaxed for final atomic structure. This superlattice can be described by a rod with alternating diameters or a nanowire with alternating wide and narrow parts.

We consider two superlattice structures, namely $Si_{138}H_{42}$ and $Si_{157}H_{64}$, which are grown in [111] and [100] directions, respectively. For the latter we investigate the surface defect and also Al and P substitutional impurities. The superlattice

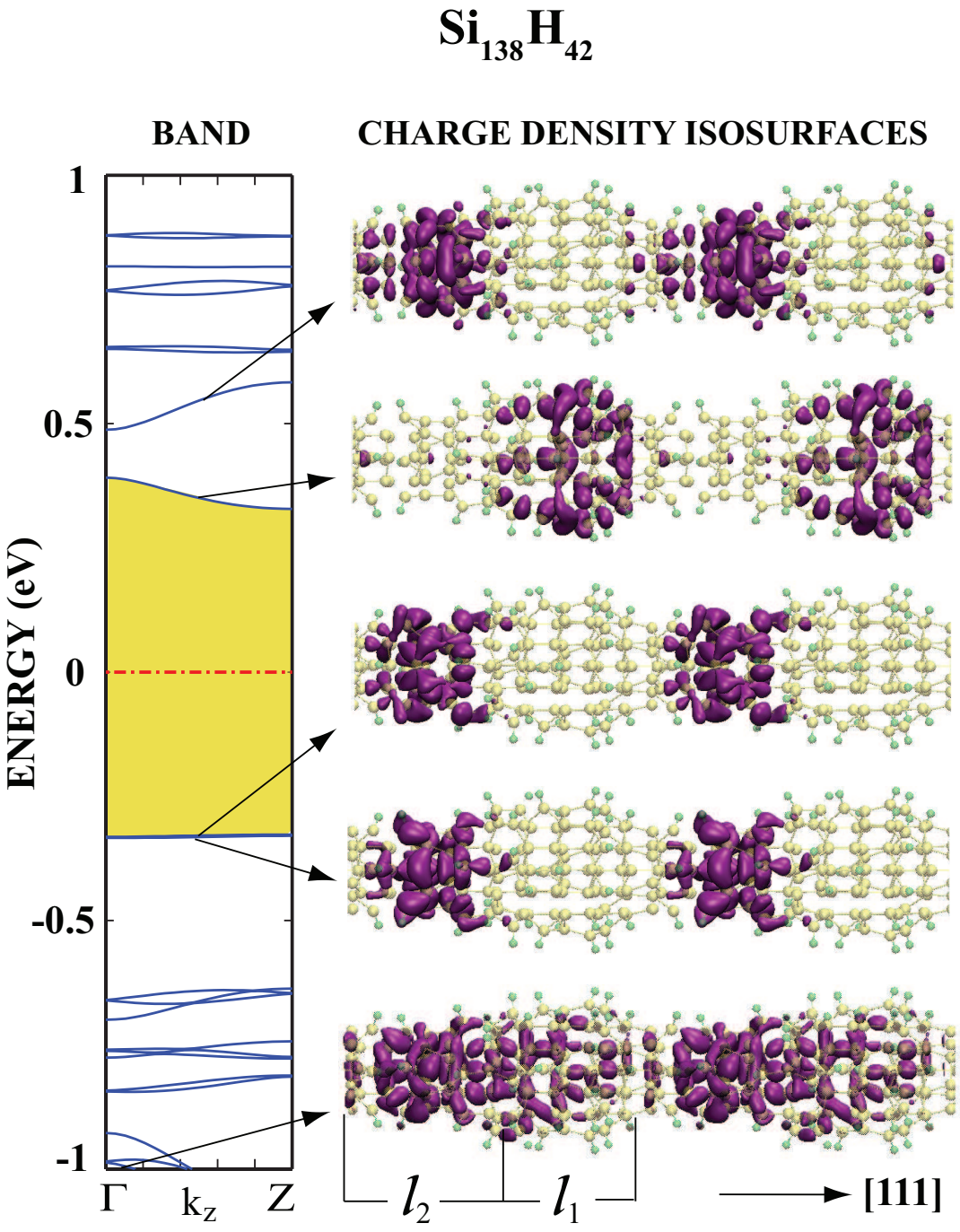

Figure 5.1: Energy band structure and charge density isosurfaces of the superlattice, $Si_{138}H_{42}$, formed from periodically repeated junctions consisting of one unit cell of SiNW with $D_1 \sim 11$ Å and two unit cell of SiNW with $D_2 \sim 7$ Å formed along [111] direction. Isosurfaces of charge density of valence and conduction band states confined at different regions in real space. Large and small balls indicate Si and H atoms. Zero of energy is set at the Fermi level shown by dash-dotted line.

$Si_{138}H_{42}$ is formed by the junction of the segments $Si_{38}H_{12}$ and $Si_{68}H_{18}$ with segment lengths of $l_1 = 1$ and $l_2 = 2$. Normally, states can propagate along the axis of the superlattice and form dispersive bands. Whereas some states can be confined to either narrow or wider parts of superlattice, if they cannot find a matching state in the adjacent part. Stated differently, if the energy of a particular state in the narrow or wide part falls in the band gap of the adjacent part, it becomes confined. Energy bands and isosurface charge density of states in specific bands are shown in Fig. 5.1. One sees propagating states, which have charge density distributed everywhere in the superlattice rod as well as states, which have high charge density in the alternating (either wide or narrow) segments. The latter types of states are identified as confined states. Defining the confinement as $\int_{l_{1,2}} |\Psi(\mathbf{r})|^2 d\mathbf{r}$, the longer the lengths of different segments, l_1 and l_2, the stronger becomes the confinement. For example, if a state is confined to the segment l_1, its confinement increases with increasing l_2, since the spill over of the confined state into the segment l_2 decreases. For perfect localization, where coupling between confined states are hindered, the segment l_1 behaves as a quantum dot. Confinement and band edge alignment in the present superlattice are reminicent of the 2D pseudomorphic or commensurate semiconductor superlattices.[41] While the states of flat degenerate band at the top of the valence band are confined in the narrow segment of the superlattice, the state at the conduction band edge is confined at the wide segment. This situation implies the staggered band alignment with confined hole states in the narrow part and confined electrons in the wide part. A state near $\sim$ -1 eV is a propagating state. Owing to short superlattice periodicity, a non-negligible coupling between confined states result in bands which exhibit minute dispersion.

Figure 5.2(a) presents the superlattice formation and confined states in a different structure, namely $Si_{157}H_{64}$ with $l_1 = 2$, $l_2 = 3$ and $D_1 \sim 14$ Å, $D_2 \sim 7$ Å formed along [100] direction. Flat minibands near the edge of conduction and valence bands are distinguished. In contrast to propagating states of dispersive bands near 1 eV, the states of these flat mini bands are confined in the narrow segments of the superlattice. This situation indicates normal band lineup. We note

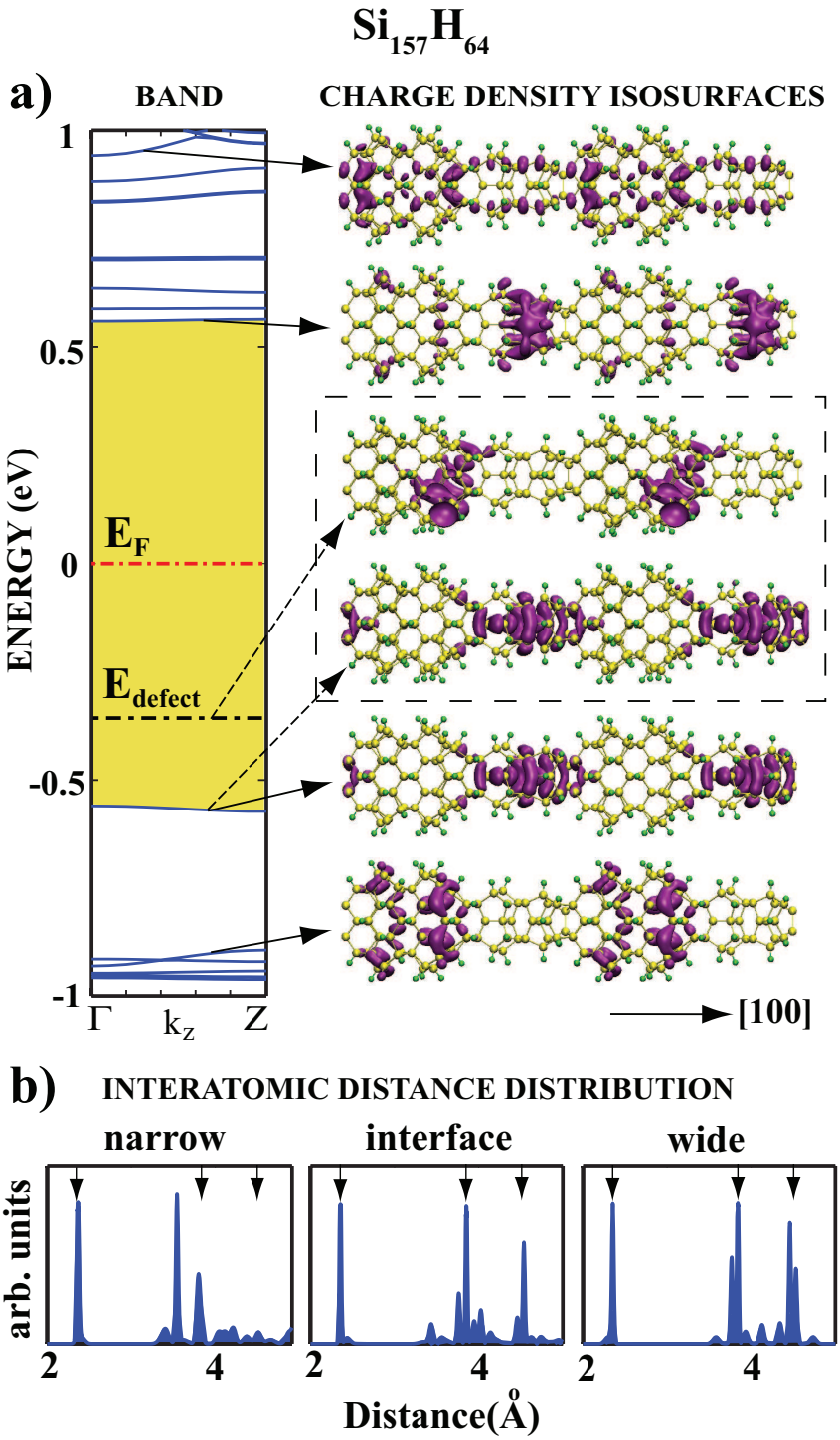

Figure 5.2: (a) Same as Fig. 5.1 for $Si_{157}H_{64}$ formed from periodically repeated junctions consisting of two unit cell of SiNW with $D_1 \sim 14$ Å and three unit cell of SiNW with $D_2 \sim 7$ Å formed along [100] direction. The charge density isosurfaces of the defect state (due to one Si and one H atom attached to it is missing from $Si_{157}H_{64}$) and the state below corresponding to the structure $Si_{156}H_{63}$ is shown in the dashed box. (b) The distribution of interatomic distances of relaxed superlattice. The arrows indicate the ideal bulk 1st, 2nd and 3rd nearest neighbor distances.

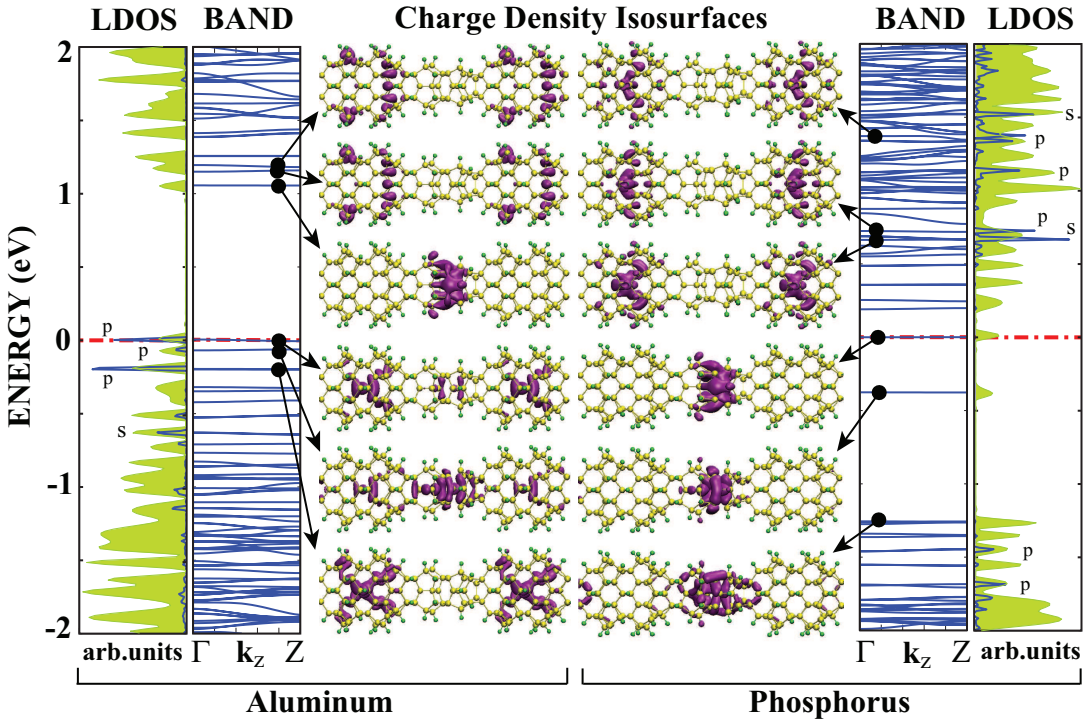

Figure 5.3: Band structure, local density of states (LDOS), charge density isosurfaces of Al and P (substitutional) doped $Si_{157}H_{64}$ (namely $Si_{156}P(Al)H_{64}$). Here, p and s indicate 3s and 3p projected LDOS at the impurity atom. Dash-dotted lines indicate the Fermi energy

that in both short periodicily superlattices discussed above the electronic structures are significantly different from the constituent SiNWs. As l_1 and l_2 increases, the superlattice effects and confined states become more pronounced, and band-offset converges to a well-defined value. For l_1 and $l_2 > \lambda_B$ (Broglie wavelength), the electronic properties in each segment becomes close to those in constituent nanowires. In addition to l_1 and l_2, D_1 and D_2 and direction of the growth are also critical parameters, since the electronic structure of the constituent SiNWs is strongly dependent on these parameters. As D_1 and D_2 increases, the surface effects decrease and the density of states becomes more bulk like. However for a significant $\Delta D = D_1 - D_2$ the superlattice effects, in particular confinement of specific states are expected to continue. In Figure 5.2(b) the distribution of interatomic distances show significant reconstruction and deformation.

Next we examine the effect of defect and doping by substitutional Al and P

impurities. A defect is created by removing one Si and one H atom and subsequently by relaxing the structure again. Odd number of electrons in this structure results in the half-filled band near the valence band edge crossing its Fermi energy. Nevertheless, this defect band changes to a localized defect level when defect-defect distance increases. As seen from the figure this state has a charge density confined around the defect, while the confined state below it, at the edge of the valence band, remains almost unchanged. The vacancy states in bulk Si are located deep in the band gap. In the superlattice structure, this vacancy state is located near the valence band since the defect is formed on the surface at the interface between two segments of different diameter.

In modulating doping, Al or P atoms are placed inside the wide part of the superlattice by substituting Si atoms. Since the superlattice has a normal band-lineup, the electrons and holes of ionized dopants shall be accommodated by the bands of states confined in the narrow parts. Energy band structure and local density of states (LDOS) are presented in Fig. 5.3. Orbital-projected LDOS identifies the origin of a particular state in terms of the orbital composition of constituent atoms. In the case of Al doping, it is clearly seen that the band gap remains unaltered, except that a state derived from the 3p orbitals of Al appears in the band gap near the valence band edge. While this Al-like state forms a band as a result of small superlattice periodicity, it becomes a localized state for large $l_1 + l_2$. The energy location and single electron deficiency of Al makes this substitutional impurity state an acceptor like state. While acceptor centers are located in the wide part of the superlattices, resulting holes are accommodated by the bands of confined states in the narrow part.

The situation in the case of P impurity is not as clear as Al. Free P atom has five valence electrons in the $3s^2 3p^3$ configuration. Since localized impurity states derived from 3p orbitals of P have occurred up in the conduction band continuum, the fifth electron of P is accommodated by the first empty conduction band originated from Si orbitals. At the end, the band gap is reduced since this half-filled band is lowered towards the band at the edge of the valence band and hence the band gap is reduced. It is noted that the half-filled band and the next lower band have almost identical charge density with the bands at the

edges of conduction and valence band of undoped $Si_{157}H_{64}$ illustrated in Fig. 5.2. It is expected that the band which overlaps with the Fermi level rises to its original position as $l_1 + l_2$ and the diameters of constituent nanowires increases. Apparently, owing to the dimensionality and size effects the donor state in the present SiNW superlattice exhibits behavior which is different from the bulk Si crystal. In particular, the hydrogenic impurity approximation can be invalidated due to the small diameter of the superlattice in the transverse direction.

Chapter 6

Metal-Semiconductor Heterostructure

In this chapter we present our results related to metal-semiconductor silicon nanowire junctions. As mentioned in previous chapters, bare silicon nanowires are metallic due to the surface dangling bond states crossing the Fermi level of the system. Saturation of these dangling bonds with hydrogen make the system semiconducting. Putting these two ingredients together one expects to get a system which contains properties similar to conventional planar metal-semiconductor junctions. The Schottky barriers that occur at the interface of these junctions result in the I-V characteristics needed for the construction of several kinds of diodes and transistors. Before running into transport calculations it is important to explore the electronic structure of metal-semiconductor nanowire junctions. We have traced the same methodology used in Chapter 4. We have chosen the silicon nanowire with smaller diameter which is composed of 25 Si atoms in the unitcell. The small diameter enables us to calculate the electronic structure of nanowires up to 8 unitcells (over 200 atoms) in it. As mentioned in Chapter 4, the superlattice effects start to get pronounced when we have 3 unitcell for each part, that is 6 unitcells in total. Normally one assumes both metal and semiconductor parts of device to be semiinfinite, but to do rigorous calculations of this structure involves somewhat sophisticated methods like Green's Function Surface

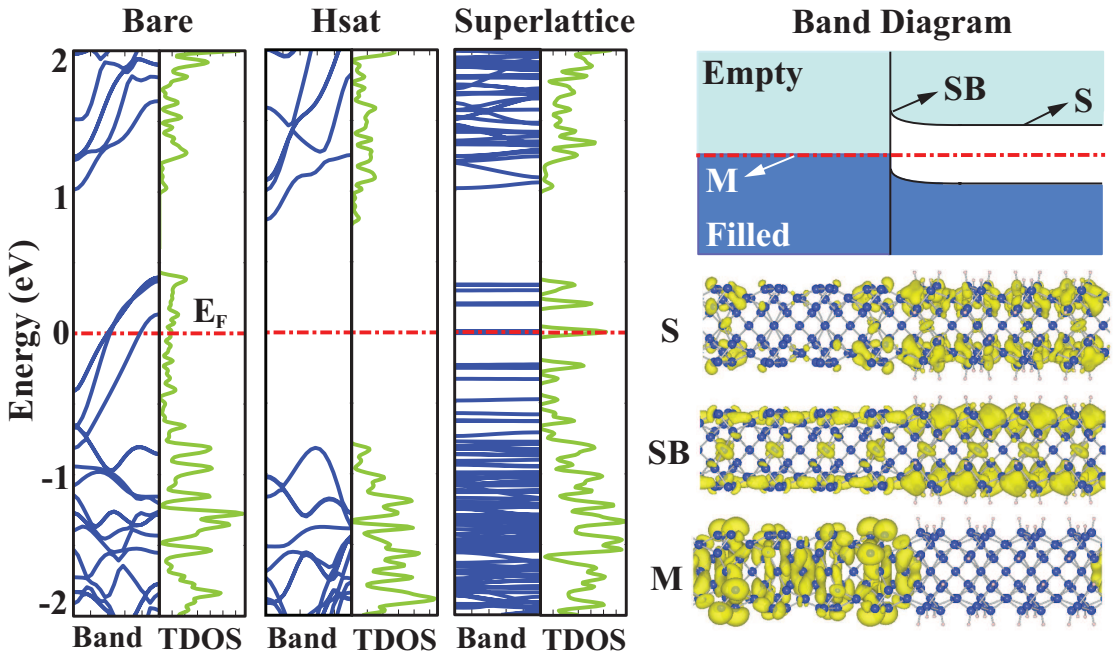

Figure 6.1: Band structure and total density of states plots for bare, hydrogen saturated and superlattice structure. Schematic diagram of band alignment in conventional metal-semiconductor junctions and charge density isosurface plots corresponding to metallic (M), semiconducting (S) and Schottky barrier (SB) states.

Matching. Instead, we have analyzed superlattice structure and tried to deduce same asymptotic trends as the length of constituent nanowires increase. Due to the computational cost we couldn't go beyond 8 unitcell, but it seems enough for making some reasonable comments.

Fig. 6.1 gives a summary of our main results. It includes band structure and total density of states (TDOS) plots for bare, hydrogen saturated and superlattice structure formed by 4 bare and 4 hydrogen saturated silicon nanowire unitcells. Aslo there is a schematic band diagram showing the Schottky barrier (SB) formation and the charge densities corresponding to some special states. One clearly see that the bare structure is metallic with three bands crossing the Fermi level, while hydrogen saturated structure has at least 1.6 eV band gap. Actually the superlattice structure also has a band gap which is so tiny that can not be seen in the figure. The peak that occur at the Fermi level of the TDOS of superlattice is a result of the sum of the smeared densities located near the Fermi level. Note also the upwards shift in the conduction band edge of the semiconducting part. This is a sign of Schottky barrier formation. The charge density corresponding to the SB state at the conduction band edge has a distribution which is spread out all over the superlattice structure. Normally, this is the conduction band state of H-saturated Si nanowire of the right hand side which is coupled with the bare Si nanowire at the left hand side. The state which is two above the SB state is denoted by S, which indicates the confined nature of this state in the semiconducting part. The state which is localized in the metallic part of the superlattice structure is denoted by M. This state gives a flat band near the fermi level.

Localization effects are also seen in shorter superlattice structures, but they are improved in larger systems. Actually, one expects that discrete density of states corresponding to localized metallic states will converge to continuous spectrum seen in its infinite counterpart. This results indicate that the pseudomorphic junction of bare and hydrogen saturated nanowires can serve as diodes and transistors in future nanoscale electronics.

Chapter 7

Conclusion

In this last chapter we present our conclusions drawn from the present thesis. Atomic structure of H-Si_n and H-Ge_n nanowires is tetrahedrally coordinated near the center, but at the surface deviates significantly from corresponding bulk crystal. Calculated force constants indicate that Si_n is stiffer than Ge_n. Generally nanowires become stiffer after passivation with hydrogen. These two nanowires are 1D semiconductors with their band gap depending on their diameter and also on the geometry of their relaxed cross section. If finite segments of these nanowires are joined pseudomorphically and the resulting heterostructure are repeated periodically along the axis of the wires, one obtains a H-Si_nGe_n superlattice structure. In these longitudinal NWSLs electrons are normally bound to the wire in radial direction, but propagate along their axis. A specific state which propagates in one zone (say H-Si) can decay in the adjacent zone (say H-Ge), when a matching state in the same energy is absent. Such a state is called confined state. Our charge density analysis indicate that Si/Ge NWSL with radius as small as 0.6 nm can have confined states at the band edges and also within the conduction and valence band. Theoretically, NWSL have several interesting issues to be clarified. In particular, theories derived from planar superlattices to predict band-lineups and model calculations using EMT have to be revised for small diameter NWSLs.

We also showed that one can form superlattices consisting of different diameters of silicon nanowires. Their band gap is modulated in real space to form 1D multiple quantum wells with confined states. These superlattices can also be suitable for modulation doping. Specifically, acceptor doping results in a localized state near the valence band edge which is similar to conventional acceptor doping. Donor doping results in the filling of valence band edge and states coming from donor atom do not occur in the band gap but rather in conduction band continua, pushing down conduction band states and lowering the band gap. At strong confinement or localization, the superlattice structures can be viewed as a series of quantum dots. Various types of electronic devices, such as resonant tunnelling double barriers generated from these superlattices, can be arranged on a single rod, where they can be connected by the metallic segments of unsaturated Si nanowires.

Finally, we showed that heterostructures formed by periodic junction of bare and hydrogenated silicon nanowires carry very similar electronic properties as one see in conventional planar metal-semiconductor junctions. The Schottky barrier formed at the interface of bare and hydrogenated zones of the nanowire, offer new options for device engineers in nanoscale.

Bibliography

[1] Jonathan E. Green *et al.*, Nature **445**, 414 (2007).

[2] Cronin B. Vining, Nature **451**, 132 (2008).

[3] Maria Telkes, J. Appl. Phys. **18**, 1116-1127 (1947).

[4] Akram I. Boukai *et al.*, Nature **451**, 168 (2007).

[5] Allon I. Hochbaum *et al.*, Nature **451**, 163 (2007).

[6] David J. Nesbitt *et al.*, Nature **450**, 1172 (2007).

[7] Vladimir Protasenko *et al.*,J. Am. Chem. Soc. **129**, 13160-13171 (2007).

[8] Jiangtao Hu *et al.*, Nature **399**, 48 (1999).

[9] M. S. Gudiksen *et al.*, Nature **415**, 617 (2002).

[10] Jie Xiang *et al.*, Nature **441**, 489 (2006).

[11] D. D. D. Ma *et al.*, Science **299**, 1874 (2003)

[12] Y. Wu, R. Fan, and P. Yang, Nano Lett. **2**, 83 (2002).

[13] J.X. Cao *et al.*, Phys. Rev. Lett. **97**, 136105 (2006).

[14] M. T. Bjork *et al.*, Nano Lett. **2**, 87 (2002).

[15] N. Wang *et al.*, Chem. Phys. Lett. **299**, 237 (1999).

[16] S.T. Lee *et al.*, J. Mater. Res. **14**, 4053 (1999).

[17] P. Hohenberg and W. Kohn, Phys. Rev. **136**, B864 (1964).

[18] W. Kohn and L. J. Sham, Phys. Rev. **140**, A1133 (1965).

[19] L. H. Thomas, Proc. Cambridge. Philos. Soc. **23**, 542 (1927).

[20] E. Fermi, Z. Phys. **48**, 73 (1928).

[21] D. R. Hartree, Proc. Cambridge. Philos. Soc. **24**, 89 (1928).

[22] V. Fock, Z. Phys. **61**, 126 (1930).

[23] J. C. Slater, Phys. Rev. **35**, 210 (1930).

[24] R. O. Jones and O. Gunnarson, Rev. Mod. Phys. **61**, 689 (1989)

[25] J. P. Perdew and Y. Wang, Phys. Rev. B, **45**, 13244 (1991).

[26] L. J. Lauhon *et al.*, Nature **420**, 57 (2002).

[27] R. N. Musin, and X-Q. Wang, Phys. Rev. **B71**, 155318 (2005).

[28] R. Kagimura *et al.*, Phys. Rev. Lett. **98**, 26801 (2007).

[29] L. C. Lew Yan Voon, and M. Willatzen, J. Appl. Phys. **93**, 9997 (2003).

[30] F. R. Zypman, Phys. Rev. **B71**, 165313 (2005).

[31] O. Gulseren, T. Yildirim and S. Ciraci, Phys. Rev. **B68**, 115419 (2003); C. Kilic, S. Ciraci, O. Gulseren and T. Yildirim, Phys. Rev. **B62**, 16345 (2000).

[32] M. C. Payne *et al.*, Rev. Mod. Phys. **64**, 1045 (1992).

[33] Numerical computations have been carried out by using VASP software: G. Kresse, J. Hafner, Phys Rev. B **47**, R558 (1993); G. Kresse, J. Furthmuller, Phys Rev. B **54**, 11169 (1996).

[34] W. Kohn and L. J. Sham, Phys. Rev. 140, A1133 (1965); P. Hohenberg and W. Kohn, Phys. Rev. B 76, 6062 (1964).

[35] D. Vanderbilt, Phys. Rev. B **41**, R7892 (1990).

[36] J. P. Perdew *et al.*, Phys. Rev. B **46**, 6671 (1992).

[37] M. Methfessel and A. T. Paxton, Phys. Rev. B **40**, 3616 1989.

[38] H.J. Monkhorst and J.D. Pack, Phys. Rev. B **13**, 5188, (1976).

[39] M. Menon *et al.*,Phys. Rev. **B70**, 125313 (2004).

[40] X. Zhao *et al.*,Phys. Rev. Lett. **92**, 236805 (2004).

[41] L. Esaki and L. L. Chang, Phys. Rev. Lett. **33**, 495 (1974).

[42] G. Bastard, Wave Mechanics Applied to Semiconductor Heterostructures (Les Editions de Physique, Les Ulis, 1988).

[43] A. K. Singh, V. Kumar, R. Note and Y. Kawazoe, Nano Lett. **6**,920 (2006).

[44] Y. Cui, Z. Zhong, D. Wang, W. U. Wang and C. M. Lieber, Nano Lett. **3**, 149 (2003).

[45] Y. Huang, X. F. Duan and C. M. Lieber, Small **1**, 142 (2005).

[46] X. F. Duan, Y. Huang, R. Agarwal and C. M. Lieber, Nature (London) **421**, 241 (2003).

[47] Y. Cui, X. F. Duan, J. Hu, and C. M. Lieber, J. Phys. Chem. B, **104**, 5213-5216 (2000).

[48] M. V. Fernandez-Serra, Ch. Adessi and X. Blase, Phys. Rev. Lett. **96**, 166805 (2006).

[49] E. Durgun, D. Cakir, N. Akman, and S. Ciraci, Phys. Rev. Lett. **99**, 256806 (2007).

[50] N. Akman, E. Durgun, S. Cahangirov and S. Ciraci, Phys. Rev. B **76**, 245427 (2007).